
1 This manuscript has been ACCEPTED for publication in JOURNAL OF GEO-
2 PHYSICAL RESEARCH: SOLID EARTH. Please note that, despite having undergone
3 peer-review, the final manuscript has yet to be edited and typeset and may be different
4 to the published version. The final version of this manuscript will be available via the
5 ‘Peer-reviewed Publication DOI’ link on the right-hand side of this webpage. Please feel
6 free to contact Bhavik.Lodhia@csiro.au; we welcome feedback.

7 **A Review of the Migration of Hydrogen from the**
8 **Planetary to Basin Scale**

9 **Bhavik Harish Lodhia, Luk Peeters, Emanuelle Frery**

10 ¹CSIRO Environment, Kensington, Perth, 6151, WA, Australia

11 ²CSIRO Environment, Waite, Adelaide, 5064, SA, Australia

12 ³CSIRO Energy, Kensington, Perth, 6151, WA, Australia

13 **Key Points:**

- 14 • History of planetary formation and overview of natural hydrogen cycle of Earth.
15 • Summary of mechanisms for hydrogen migration (diffusion and advection), gen-
16 eration and consumption by microbial reactions.
17 • Summary of indicative timescales of hydrogen migration within crystalline and sed-
18 imentary rocks.

Corresponding author: Bhavik Harish Lodhia, Bhavik.Lodhia@csiro.au

Abstract

The occurrence of natural hydrogen and its sources have been reviewed extensively in the literature over the last few years, with current research across both academia and industry focused on assessing the feasibility of utilising natural hydrogen as an energy resource. However, gaps remain in our understanding of the mechanisms responsible for the large-scale transport of hydrogen and migration through the deep and shallow Earth and within geological basins. Due to the unique chemical and physical properties of hydrogen, the timescales of migration within different areas of Earth vary from billions to thousands of years. Within the shallow Earth, diffusive and advective transport mechanisms are dependent on a wide range of parameters including geological structure, microbial activity, and subsurface environmental factors. Hydrogen migration through different media may occur from geological timescales to days and hours. We review the nature and timescale of hydrogen migration from the planetary to basin-scale, and within both the deep and shallow Earth. We explore the role of planetary accretion in setting the hydrogen budget of the lower mantle, discuss conceptual frameworks for primordial or deep mantle hydrogen migration to the Earth's surface and evaluate the literature on the lower mantle's potential role in setting the hydrogen budget of rocks delivered from the deep Earth. We also review the mechanisms and timescales of hydrogen within diffusive and advective, fossil versus generative and within biologically moderated systems within the shallow Earth. Finally, we summarise timescales of hydrogen migration through different regions within sedimentary basins.

Plain Language Summary

Over the last several years, naturally-occurring hydrogen has emerged as a potential game changer in the energy transition. However, the vast majority of current research focuses on understanding hydrogen generation and underground storage. Important questions remain - how did hydrogen come to be within Earth? What are the timescales of hydrogen movement through different regions of Earth and within different rock types? In this review, we describe the processes responsible for entraining hydrogen into Earth's mantle during the time of planetary formation and timescale of evolution towards the present-day hydrogen cycle. We summarise the importance of environmental factors and mineralogy for hydrogen movement and the timescale of generative and destructive processes in the shallow Earth. Finally, we summarise the timescale of hydrogen movement within different regions of Earth from the planetary to basin-scale and within different minerals and rock types.

1 Introduction

Hydrogen is regarded as an important component of the world's transition towards a low emission, net-zero future (IEA, 2021). Significant efforts are currently being made across academia and industry to improve our understanding of hydrogen subsurface mobility, especially in the context of natural hydrogen occurrence and underground storage (e.g., Zgonnik (2020); Muhammed et al. (2022); L. Wang, Jin, et al. (2023)). Within the literature, the term 'natural hydrogen' describes the hydrogen which is not manufactured and is directly found in the subsurface. Natural Hydrogen is encountered as a free gas (i.e., surface seeps), dissolved in groundwater and within fluid inclusions in rocks. Natural hydrogen migrates through a wide range of mechanisms, including diffusion (e.g., through crystalline lattices) and advection (e.g., dissolution in groundwater, migration along faults) (e.g. Farver (2010); Lefeuvre et al. (2021, 2022); Strauch et al. (2023); Truche et al. (2024)). Whilst laboratory experiments and assessments of specific case studies have shed some light on the complex nature of natural hydrogen migration, large gaps remain in our understanding of the mechanisms responsible for the large-scale migration of hydrogen through the deep Earth and within sedimentary basins. In this review, we refer

69 to the regions beneath the lithosphere, i.e. mantle, as the ‘deep’ Earth, and subsurface
70 regions within geological and sedimentary basins as the ‘shallow’ Earth.

71 This review overviews the processes responsible for setting Earth’s hydrogen bud-
72 get and the timescales of hydrogen migration across all length-scales within Earth. We
73 review (i) the origin of primordial or deep mantle natural hydrogen supply to the deep
74 Earth, the role of water on mantle mixing and Earth’s hydrogen cycle over geological timescales
75 and (ii) the dynamics of diffusive and advective hydrogen migration within the shallow
76 Earth on geological to human timescales.

77 2 Hydrogen in the deep Earth

78 Whilst hydrogen is the most abundant element in the universe, molecular hydro-
79 gen is scarce on Earth. Estimates of the hydrogen abundance in Earth’s interior have
80 spanned a range from less than the equivalent of the current hydrosphere to on the or-
81 der of 100 hydrospheres if hydrogen is the dominant light alloying component in Earth’s
82 outer core (Williams & Hemley, 2001). There is a limited understanding of its sources,
83 migration through rocks and whether hydrogen can accumulate in geological formations
84 for significant time periods. To understand the nature of hydrogen migration within Earth,
85 we must first consider its origins and distribution on a planetary scale. Within the deep
86 Earth, there exist reservoirs of primordial or deep mantle hydrogen trapped during the
87 period of planetary formation, which are proposed by some models to be transported by
88 advection within the mantle on timescales of billions of years (Peslier et al., 2017; Loewen
89 et al., 2019). For a detailed description of the mineralogical composition and hydrogen
90 content of the deep Earth, see Williams and Hemley (2001). Following planetary accre-
91 tion, the stabilisation of liquid water on the surface and onset of plate tectonics had a
92 profound impact on the dynamics of mantle flow and Earth’s hydrogen cycle. This in-
93 cludes the contamination of non-native material into Earth’s mantle at subduction zones
94 and its heterogeneity in mantle hydrogen contents. Conversely, the preservation of iso-
95 topic signatures indicate that mantle material delivered to Earth’s surface at hotspot set-
96 tings preserve their deep mantle or primordial isotopic signatures and do not mix with
97 surrounding mantle (Mangenot et al., 2023). The timescale of hydrogen transport from
98 within the deep Earth to different geological settings at the surface vary across several
99 orders of magnitude. In this section, we describe the discrepancies between hydrogen and
100 helium isotopic ratios encountered in rocks from different geological settings and com-
101 pare frameworks for hydrogen migration to the Earth’s surface from the deep mantle.

102 Global hydrogen cycle

103 Whilst up to 90% of the proto-solar nebula comprised of hydrogen, ^1H , the isotopes
104 deuterium, ^2H , and Helium-3, ^3He , were also created during the Big Bang. Unlike ter-
105 restrial ^4He , which is mainly produced by decay of uranium and thorium, terrestrial ^3He
106 is largely of primordial origin, synthesised in the aftermath of the Big Bang (Bania et
107 al., 2002) and incorporated into the Earth primarily during its formation (Lupton & Craig,
108 1975). In spite of its primordial status and 4.56 Ga of planetary evolution, up to ~ 2
109 kg ^3He continues to leak from Earth’s interior and mainly along mid ocean ridges (Olson
110 & Sharp, 2022). The reference proto-solar D/H ratio is $\sim 2.1 - 2.5 \times 10^{-5}$, which is
111 close to the Big Bang value. Due to its mass, hydrogen is lost through diffusion prefer-
112 entially over deuterium and the D/H ratio increases with geologic time. As ^4He is a de-
113 cay product of U-Th-Pb α -decay systems, $^3\text{He}/^4\text{He}$ ratios with Earth decrease mono-
114 tonically with time, with high $^3\text{He}/^4\text{He}$ rocks indicating preservation in mantle domains
115 that are not modified by convective mixing or diffusive homogenisation since early Earth
116 history (Porcelli & Elliott, 2008; Huang et al., 2014; Cooke et al., 2014; Lis et al., 2019).
117 The reaction of deuterium, hydrogen and water, $\text{HD} + \text{H}_2\text{O} \rightleftharpoons \text{H}_2 + \text{HDO}$, is an impor-
118 tant measure of the thermal history of water molecules since the formation of Earth. The

124 Mid Ocean Ridges are transform margins where upwelling mantle is extruded at
 125 Earth's surface to form new oceanic crust. Mid-Ocean Ridge Basalts (MORBs) are mafic
 126 rocks derived from larger mantle domains that appear to sample deep mantle hydrogen
 127 transported to the melting domain in the upper mantle by large-scale mantle convection
 128 and typically have low δD values of $\sim -70\%$ (Table 1) (Craig & Lupton, 1976; Rison
 129 & Craig, 1983; Poreda et al., 1986; Graham, 2002; Jackson et al., 2017; Loewen et al.,
 130 2019). $^3\text{He}/^4\text{He}$ ratios in MORBs are typically homogeneous and have a narrow range
 131 of $7 - 9 R_A$, whereby R_A = atmospheric ratio (C. J. Allègre et al., 1995; Gautheron
 132 & Moreira, 2002). Helium ratios analysed in MORB glasses by C. J. Allègre et al. (1995)
 133 from individual ridge segments show a linear correlation with the ridge spreading rate.
 134 Average helium ratios of MORBs are predominantly uniform and distinct from lower man-
 135 tle and transition zone values, which is interpreted by C. J. Allègre et al. (1995) to in-
 136 dicate the existence of two scale upper mantle convection. Rapid convection within the
 137 uppermost mantle that feeds mid ocean ridges (see red arrows on Figure 1) is respon-
 138 sible for the homogenisation of helium in this layer and is calculated to have a mixing
 139 time of ~ 250 Ma, which is distinct from the ~ 1 Ga residence time of upper mantle
 140 rocks (C. Allègre et al., 1983; C. J. Allègre et al., 1995) (Figure 1).

141 Whilst enriched compared to non-mantle rocks, helium ratios in MORBs are sig-
 142 nificantly less than those found at Ocean Island Basalt (OIB) and Continental Hotspot
 143 (CH) settings, which can reach values $< 40R_A$ (Table 1). Although the nature of plume
 144 development over geological time remains an active topic of research, it is widely accepted
 145 that mantle plumes which feed OIB and CH settings may extend as deep as the core/mantle
 146 boundary (~ 2900 km) (Figure 1). Plumes that transport lower mantle rocks with high
 147 $^3\text{He}/^4\text{He}$ and low δD signatures that are enriched in deep mantle water, i.e. water that
 148 has never been present at Earth's surface, are significant as they are conduits of deep
 149 mantle hydrogen and helium entrained in ultramafic rocks that are extruded at Earth's
 150 surface. Recent investigations into the architecture of hotspot-plume systems suggest that
 151 material transported via hotter and more buoyant mantle plumes have increased resilience
 152 to mixing with surrounding mantle and increased preservation of deep mantle geochem-
 153 ical signatures compared to colder and less buoyant plumes (Samuel & Farnetani, 2003;
 154 S. C. Lin & Keken, 2006; Garnero et al., 2016; Jackson et al., 2017; Jimenez-Rodriguez
 155 et al., 2023). It is noteworthy that CH settings exhibit δD values close to MORB, how-
 156 ever $^3\text{He}/^4\text{He}$ ratios are significantly higher ($< 20 R_A$). Some, like the African hotspots,
 157 also have δD values as low as -89% (Table 1) (Jimenez-Rodriguez et al., 2023). Further-
 158 more, experimental results from Mangenot et al. (2023) indicate that H_2 is sensitive to
 159 isotope re-equilibration (e.g. between H_2 and water at its source) during the ascent and
 160 cooling of high-temperature crustal, magmatic, and mantle fluids. These observations
 161 indicate that material transport from the lower mantle must be fast enough to prevent
 162 mixing with both upper mantle and the surrounding continental cratonic rocks and sig-
 163 nificantly faster than the timescale upper mantle mixing. Hence, we hypothesise that the
 164 degree of enrichment of deep mantle hydrogen and helium within rocks delivered to OIB
 165 and CH settings, and therefore their surrounding terrestrial environments through sub-
 166 surface processes e.g. serpentinisation, is controlled by the rate at which rocks are sup-
 167 plied from lower mantle reservoirs. This must be on the timescale of, at least, millions
 168 of years instead of hundreds of millions of years. Thus, the timescale of migration of rocks
 169 enriched in hydrogen from within the deep Earth varies over several orders of magnitude
 170 between different geological regimes and is distinct from water residence times.

171 Hence, it is likely that whilst the background flux of primordial or deep mantle hy-
 172 drogen to upper mantle regions which supply melt to Mid Ocean Ridges is set by large-
 173 scale mantle convection over billions of years, the mixing of primordial or deep mantle
 174 hydrogen and helium-enriched material into the upper mantle is an order of magnitude
 175 faster over hundreds of millions of years.

176

Primordial versus deep mantle hydrogen and helium ratios

177

178

179

180

181

182

183

184

185

186

187

188

189

190

191

192

193

194

Although the primordial origins of ^3He are generally accepted, there is controversy within the scientific community regarding application of $^3\text{He}/^4\text{He}$ ratios as a diagnostic marker for primordial material. The value of the $^3\text{He}/^4\text{He}$ ratio from the local interstellar medium (LISM) is $1.7 \pm 0.8 \times 10^{-4}$, and is around two orders of magnitude greater than the present-day atmospheric value, $R_A = 1.4 \times 10^{-6}$ (Graham (2002); Salerno et al. (2003), see Table 1). LISM values are consistent with protosolar ratios obtained from meteorites and Jupiter’s atmosphere, supporting the hypothesis that negligible changes of the abundance of ^3He occurred in the galaxy during the past 4.5 Ga (Salerno et al., 2003). High $^3\text{He}/^4\text{He}$ ratios in Ocean Island Basalts (OIBs) were traditionally interpreted as indicators of a primitive, undegassed mantle source that has been trapped within the Earth to the present day (Bouhifd et al., 2013). This interpretation was predicated on the assumption that these ratios reflect the composition of material sampled by rapidly ascending thermally buoyant plumes arising from deep within the mantle (Kurz et al., 1982; Morgan, 1971; Kellogg & Wasserburg, 1990). Despite this established view, primordial models fail to account for observed discrepancies in helium concentrations and the elemental ratios of He and other noble gases (e.g. Ar and Ne) between OIBs and Mid-Ocean Ridge Basalts (MORBs), with the former displaying values an order of magnitude lower than those found in MORBs (Gonnermann & Mukhopadhyay, 2007).

195

196

197

198

199

200

201

202

203

204

205

The debate over the origins of high $^3\text{He}/^4\text{He}$ ratios in OIBs and how these ratios address the helium paradoxes has been extensively explored in the literature. Gonnermann and Mukhopadhyay (2007) present a model in which the helium concentration paradox, as well as the variance in noble-gas concentrations observed in MORB and OIB glasses, can be explained by disequilibrium open-system degassing of erupting magma. Their work suggests that higher CO_2 content in OIBs leads to more extensive helium degassing in OIB magmas compared to MORBs, thus deriving noble gases in OIB lavas from a largely undegassed primitive mantle source. This interpretation aligns with the conventional view that high $^3\text{He}/^4\text{He}$ ratios in OIBs indicate parts of the deep mantle have remained isolated from outgassing and the convective upper mantle over Earth’s history (Gonnermann & Mukhopadhyay, 2007).

206

207

208

209

210

211

212

213

214

215

216

217

218

219

Bouhifd et al. (2013) assess helium partitioning in experiments between molten silicates and iron-rich metal liquids at conditions representative of Earth’s lower mantle and core. Their results and estimated concentrations of primordial helium suggest that significant quantities of helium may reside in the core and that the early core could have incorporated enough helium to supply deep-rooted plumes enriched in ^3He throughout Earth history. Bouhifd et al. (2013) therefore suggest that two variations in the $^3\text{He}/^4\text{He}$ ratio observed at the surface in OIBs and MORBs may be explained by two distinct reservoirs in the Earth’s interior (e.g. Hopp and Tieloff (2008)). These are a conventional depleted mantle source and a deep, still enigmatic, source that must have been isolated from processing throughout Earth history. However, modelling of helium ingassing into a silicate magma ocean and iron-rich proto-core coupled to a nebular atmosphere of solar composition and outgassing into a coupled core-mantle system after accretion by Olson and Sharp (2022) indicates that Earth’s core may be a substantial and long-lived reservoir of primordial helium.

220

221

222

223

224

225

226

227

228

Zhu et al. (2020), however, offer a contrasting perspective by proposing that helium contents and $^3\text{He}/^4\text{He}$ isotopic ratios can be fractionated by thermal diffusion in the lower mantle, driven by an adiabatic or convective temperature gradient. Their model suggests that the lower mantle is helium stratified due to thermal diffusion, resulting from a of ~ 400 K temperature contrast across the lower mantle. Hence, Zhu et al. (2020) argue that helium fractionation, rather than the lower mantle being a primordial and undegassed reservoir, explains the observed high $^3\text{He}/^4\text{He}$ isotopic ratios and lower helium contents in OIBs. Zhu et al. (2020) argue that OIBs derived from the deepest lower mantle, which display high $^3\text{He}/^4\text{He}$ isotopic ratios and less helium content, can be ex-

229 plained by their model, effectively addressing the long-standing helium concentration para-
 230 dox without necessitating a primordial undegassed lower mantle reservoir.

231 These differing viewpoints illustrate the complexity of mantle dynamics and the
 232 origins of helium isotopic variations and their implications for characterising truly pri-
 233 mordial source material. It is beyond the scope of this review to explore this subject in
 234 greater detail, however it is widely accepted that isotopic signatures may be used to di-
 235 agnose the preservation of deep lower mantle material over geologically significant time
 236 periods transported rapidly over planetary length scales (e.g., Mackintosh and Ballen-
 237 tine (2012)). However, whilst the influence of primordial material on rocks that preserve
 238 high $^3\text{He}/^4\text{He}$ isotopic signatures rocks are debated, we acknowledge that this cannot
 239 be excluded entirely.

240 **The impacts of water on the deep Earth and early tectonics**

241 As isotopic signatures of igneous rocks may be used to identify material sourced
 242 from deep lower mantle reservoirs, they offer an insight into the hydrogen cycle of the
 243 deep Earth. Whilst the diffusion of water and hydrogen in silicates is fast compared to
 244 other elements, it cannot explain the heterogeneity of lower mantle material or enrich-
 245 ment within rocks delivered by mantle plumes or upwelling. In the absence of water in-
 246 filtration into the deep mantle, mantle convection alone would lead to homogeneous wa-
 247 ter contents among regions of more than ~ 100 km size (Peslier et al., 2017). For typ-
 248 ical asthenospheric conditions, diffusion of hydrogen over a distance of ~ 10 km takes
 249 ~ 1 Ga (Karato, 2007; Peslier & Bizimis, 2015; Peslier et al., 2017). Estimates of the
 250 residence time of water within different layers in Earth are calculated by Bodnar et al.
 251 (2013) as < 3000 years for the hydrosphere, $0.77 - 7$ Ma (million years) for the litho-
 252 sphere and \sim Ga (billion years) for the transition zone and lower mantle (Figure 1).

253 Combined evidence from several radionuclide systems (Pd-Ag, Mn-Cr, Rb-Sr, U-
 254 Pb) suggests that water was not incorporated in Earth in significant quantities until the
 255 planet had grown to $\sim 60 - 90\%$ of its current size, while core formation was still on-
 256 going (Peslier et al., 2017). Prior to the onset of plate tectonics, some models propose
 257 that the early Earth lost heat generated from planetary accretion and radioactive de-
 258 cay of isotopes in the metallic core through degassing and volcanism according to a stag-
 259 nant or mobile lid regime during the late Hadean (Solomatov & Moresi, 2000; Capitanio
 260 et al., 2022). The fractionation of Earth into the core, mantle and early crust is proposed
 261 by those models to have created a stratified water structure within the planet. During
 262 this period, photolysis from solar radiation and late crust-forming events led to signif-
 263 icant loss of water from the early crust and upper mantle, leading to the lower mantle
 264 becoming relatively enriched in primordial or lower mantle water, hydrogen and helium
 265 (Peslier et al., 2017). The gradual accumulation of liquid water oceans is generally ac-
 266 cepted to be a result of the impact of chondritic material from the asteroid belt follow-
 267 ing the period of heavy bombardment and stabilisation of Earth's late veneer. Depend-
 268 ing on which estimates are used for the water and carbon contents of the bulk silicate
 269 Earth, $20 - 100\%$ of the early mantle's hydrogen and carbon may have been brought
 270 to Earth by carbonaceous chondrites during this late stage of planetary formation (Marty
 271 & Yokochi, 2006; Z. Wang & Becker, 2013; Marty, 2012; Peslier et al., 2017; Loewen et
 272 al., 2019).

273 The earliest known evidence for liquid water present on Earth's surface includes
 274 the Isua Greenstone Belt, where pillow-lava structures consistent volcanic eruption in
 275 submarine conditions occur as early as ~ 3.8 billion years ago (Polat & Hofmann, 2003).
 276 The presence of stable liquid water on Earth's surface marks a significant point in ge-
 277 ological history, as the infiltration of water-rich mineral phases into the upper mantle
 278 reduced melting temperatures and led to the formation of the mechanically weak Astheno-

Setting	δD [‰]	$^3\text{He}/^4\text{He}$ [R_A]	Example	Reference
OIB	< -75	< 40	Iceland, Hawaii Samoa, Galapagos Easter	(Jackson et al., 2017) (French & Romanowicz, 2015) (Boschi et al., 2007) (Poreda et al., 1986) (Rison & Craig, 1983)
MORB	-70^*	$7 - 9$	Iceland Mid Atlantic Ridge	(C. J. Allègre et al., 1995) (Gautheron & Moreira, 2002)
Arc/back-arc	-20 to -40^{**}	$\sim 1^{***}$	Valu Fa ridge Andes	(Hilton et al., 1993)
CH	-23 to -89	$8 - 20$	Afar, Darfur Hoggar	(Jimenez-Rodriguez et al., 2023) (Jackson et al., 2017)

Table 1. Typical isotope ratios of various tectonic settings. OIB = Ocean Island Basalt, MORB = Mid Ocean Ridge Basalt, CH = Continental hotspot. δD values are measured relative to Standard Mean Ocean Water (see text). $^3\text{He}/^4\text{He}$ ratios are measured relative to present-day atmospheric values, R_A , where $R_A = 1.4 \times 10^{-6}$ (Graham, 2002). OIB settings supported by hotter mantle plumes with increased buoyancy are hypothesised to support increased transport of primordial or deep mantle material from the lower mantle to Earth’s surface (Jackson et al., 2017). *Extremely low δD values of < -90 ‰ are observed in some MORBs associated with multi-stage melting and anhydrous minerals isotopic fractionation (see text) (Loewen et al., 2019). **High δD values in typical arc and back-arc settings (< -20 ‰) indicate the recycling of non-mantle water due to the subduction of hydrous minerals contained in the mantle wedge from beneath arc lavas, with lower δD values (> -40 ‰) associated with mixing with depleted mantle sources (Shaw et al., 2008). ***Igneous rocks from arc/back-arc settings not associated mantle mixing (i.e. differentiated silicic rocks) have negligible $^3\text{He}/^4\text{He}$ ratios $\sim 1R_A$ (Hilton et al., 1993). Continental hotspots, most notably African examples, vary significantly from continental lithosphere and differentiated back-arc basin igneous rocks. Mantle-supported continental hotspot have $^3\text{He}/^4\text{He}$ ratios ranging from typical MORB values to $20R_A$ (Jackson et al., 2017).

279 sphere, and the onset of plate tectonics around ~ 3 billion years ago (Farquhar et al.,
280 2002; Shirey & S.H., 2011; Debaille et al., 2013).

281 Since both helium and hydrogen are incompatible during mantle melting (i.e. both
282 partition into a melt as soon as melting begins), high $^3\text{He}/^4\text{He}$ ratios characterise a man-
283 tle that has been isolated from melting and degassing since the earliest stages of Earth
284 history (C. Allègre et al., 1983; Mukhopadhyay, 2012; Loewen et al., 2019). Hence, rocks
285 which contain low δD and high $^3\text{He}/^4\text{He}$ signatures are a prime target for understand-
286 ing sources of deep mantle water that has survived significant mixing and transport over
287 planetary lengthscales (Craig & Lupton, 1976; Rison & Craig, 1983; Poreda et al., 1986;
288 Loewen et al., 2019; Mackintosh & Ballentine, 2012).

289 Subduction zones represent the primary regions of terrestrial water exchange be-
290 tween Earth’s interior and hydrosphere. It is estimated that $\sim 25\%$ of the water enter-
291 ing subduction zones reaches the transition zone and $\sim 3\%$ reaches the lower mantle through
292 transport via lithosphere fragments (LF) that separate from subducted slabs (Figure 1)
293 (Bodnar et al., 2013). Slab break-off and the transport of lithosphere fragments to the
294 deep mantle has been investigated extensively, and is supported by plate tectonic recon-
295 structions and geophysical data (e.g. (Williams & Hemley, 2001; Sperner et al., 2001;
296 Zahirovic et al., 2016; Kufner et al., 2021)). It is impossible to know the precise amount

297 of lithospheric material that has been returned to the mantle over geologic time, how-
 298 ever it is reasonable to imagine the presence of graveyards of remnant fossil lithosphere
 299 distributed heterogeneously throughout the mantle (e.g., van der Meer et al. (2018)).

300 The subduction of hydrous minerals and recycling of water into the mantle over
 301 geologic time and to the present day thus led to an increase in δD in Earth's crust, up-
 302 per mantle, oceans and atmosphere compared to primitive or lower mantle materials. Es-
 303 timates of the water content within Earth range from 7–14 M_{oceans} within the man-
 304 tle and $< 12 M_{oceans}$ in the core (Bodnar et al., 2013; Nestola & Smyth, 2016; Peslier
 305 et al., 2017). Hence, subduction and lithosphere fragments have a profound impact on
 306 the dynamics of mantle convection and Earth's hydrogen cycle through mixing of
 307 non-mantle material into deep mantle reservoirs.

308 As Earth's crust and tectonic processes evolved, the planet's atmosphere also un-
 309 derwent significant changes that impacted the stability of water and hydrogen genera-
 310 tive processes on Earth's surface. Dodd et al. (2022) investigated hydrogen dynamics be-
 311 fore and after the Great Oxidation Event (GOE) at $\sim 2.5 - 2.0$ Ga. Initially, abiotic
 312 reactions in anoxic conditions led to hydrogen generation from banded iron formations
 313 (BIFs), with free hydrogen escaping due to low oxygen levels. As the concentration of
 314 biologically generated O_2 within Earth's atmosphere gradually increased, the atmosphere
 315 changed from weakly reducing conditions and practically devoid of oxygen into oxidis-
 316 ing conditions, and containing abundant free oxygen Torres et al. (2015). Post-GOE, el-
 317 evated oxygen facilitated water formation by reacting with hydrogen, reducing hydro-
 318 gen escape and transitioning Earth to a more oxidised state supportive of aerobic life and
 319 altering geochemical dynamics significantly (Dodd et al., 2022).

320 Present-day patterns of high-angle subduction and mantle wedge hydration (i.e.
 321 as shown on Figure 1) were not dominant during the early Earth, as most present-day
 322 subduction initiation mechanisms require acting plate forces and existing zones of litho-
 323 spheric weakness, which are both consequences of plate tectonics. In the absence of plate
 324 tectonic-related subduction, mechanisms responsible for the initiation of tectonics dur-
 325 ing early history are theorised to be plume-induced subduction, which is only feasible
 326 in the hotter early Earth for old oceanic plates. In contrast, younger plates favoured episodic
 327 lithospheric drips rather than self-sustained subduction and global plate tectonics (Gerya
 328 et al., 2015). It is possible that the development of the modern, globally interconnected
 329 plate network and subduction-related tectonics did not arise until billions of years af-
 330 ter the formation of the earliest crust and as late as Proterozoic times (Wan et al., 2020).
 331 This assertion is consistent with modeling studies that demonstrate that much of the con-
 332 tinental crust of Archean cratons could have been generated in the absence of subduc-
 333 tion (Capitanio et al., 2019; Johnson et al., 2017).

334 However, some evidence indicates localised infiltration of hydrated mantle wedges
 335 into the mantle occurred as early as 3.1 Ga, there is a consensus in the literature that
 336 higher mantle temperatures, lower mantle viscosity and the subduction or infiltration
 337 of oceanic crust at an unusually low angle was responsible for the growth of continen-
 338 tal crust older than ~ 2.5 Ga (e.g., Perchuk et al. (2023); Smithies et al. (2003)). Al-
 339 though, it is important to note that a hotter mantle would lead to lower viscosity and
 340 thus more melt, with the lower viscosity leading to more frequent slab breakoff, and to
 341 increased crustal separation from the mantle lithosphere (van Hunen & van den Berg,
 342 2008). Crustal and lithospheric fragments which break off, contaminate, and sink into
 343 the mantle raise δD and lower $^3He/^4He$ ratios over geologic time away from primordial
 344 or lower mantle values and towards their present-day values. Therefore, it is our view
 345 that whilst localised tectonic processes early in Earth history will have had some impact
 346 on the distribution of hydrogen within the mantle, the onset of global subduction marked
 347 the turning point of large-scale mantle mixing leading to present-day heterogeneous man-
 348 tle hydrogen contents. Throughout Earth history, plume-related tectonics will have been

349 responsible for transporting material enriched in primordial or lower mantle hydrogen
 350 and helium to the surface on geologically short timescales.

351 **3 Hydrogen in the shallow Earth**

352 Whilst the migration of hydrogen in the deep Earth is dependent on large-scale man-
 353 tle convective and tectonic processes that operate from billions to millions of years, the
 354 enrichment of hydrogen within near-surface systems and ongoing emission from surface
 355 seeps across the globe represents an intriguing duality of length-scales and timescales.
 356 Shallow Earth processes, such as the migration in porous media, migration along faults
 357 and fractures and microbial reactions may operate over timescales of thousands of years
 358 to hours. To understand hydrogen migration in the shallow Earth, we must acknowledge
 359 the relationship between hydrogen sources and transport mechanisms at the crustal, basin
 360 and outcrop scale, i.e. $10^3 - 1$ m. The primary mechanisms of natural hydrogen gener-
 361 eration are thought to be: (1) serpentinisation of mafic rocks, (2) radiolysis of water, (3)
 362 rock fracturing and (4) volcanic degassing, (5) maturation of organic matter and (6) weath-
 363 ering of iron-rich rocks (Takai et al., 2004; Klein et al., 2013; Zgonnik, 2020; Lefeuvre
 364 et al., 2021, 2022; Geymond et al., 2022; Horsfield et al., 2022; Mahlstedt et al., 2022;
 365 Boreham et al., 2023; Lévy, Roche, et al., 2023; L. Wang, Jin, et al., 2023).

366 However, to date a distinction between processes that release primordial or deep
 367 mantle (i.e. fossil) hydrogen and the chemical and biological production/destruction of
 368 ‘new’ hydrogen is seldom made in the literature. Hydrogen gas concentrations of $> 10\%$
 369 have been encountered in various locations across different tectonic regimes (see Zgonnik
 370 (2020)) with one documented case of a successful resource discovery in Mali (Prinzhofer
 371 et al., 2018). The mineralogies of Archaen - Proterozoic basement rocks in continental
 372 cratonic regions (e.g. Africa, Brazil, Russia) and mantle-derived rocks (e.g. MORBs, OIBs)
 373 are enriched in hydrogen. Hence, within the continental realm, regions of high hydro-
 374 gen concentration coincide with sedimentary basins underlain by Archean - Proterozoic
 375 cratonic rocks enriched in hydrogen (Zgonnik, 2020; Moretti, Brouilly, et al., 2021). Early
 376 estimates of global hydrogen production rates via both radiolysis and hydration reac-
 377 tions from the Precambrian continental lithosphere were reported at $0.36 - 2.27 \times 10^{11}$
 378 moles/year and are comparable to estimates from marine systems (Lollar et al., 2014).
 379 As recent literature has reviewed the topic of natural hydrogen generation extensively
 380 (e.g. Zgonnik (2020); Moretti, Brouilly, et al. (2021); L. Wang, Jin, et al. (2023)), we limit
 381 our coverage of this topic and focus on the relationship between natural hydrogen gener-
 382 eration and its migration pathways to Earth’s surface. In this section, we review the mech-
 383 anisms and timescales of transport of hydrogen within diffusive and advective systems,
 384 including transport along faults and microbial reactions, within the shallow Earth.

385 **Diffusion**

386 *Diffusion in crystalline rocks and minerals*

387 Diffusive mechanisms transport hydrogen without any motion of a material’s bulk
 388 (e.g. rock, crystalline matrix or fluid). Experimental results of hydrogen diffusivity within
 389 crystalline rocks are reviewed extensively by Farver (2010); Demouchy (2010); Li and
 390 Chou (2015) (see references therein) and summarised in Figure 2. Within the primary
 391 mafic rock-forming minerals olivine, pyroxene and amphibole, the Arrhenius plots of Farver
 392 (2010) indicate a pattern of decreasing hydrogen diffusivity from 10^1 cm^2/year to 10^1
 393 $\text{mm}^2/10$ ka with decreasing Mg content. Hydrogen diffusivity within quartz and feldspar
 394 vary between 10^1 cm^2/year to 10^1 cm^2/ka , however have been measured up to 1 m^2 yr^{-1}
 395 - 1 m^2 day^{-1} in the case of fused quartz at temperatures > 1200 K (Li & Chou, 2015).
 396 Oxide minerals, which are significant components of soils and regolith, along with meta-
 397 morphic minerals (e.g. garnet) have hydrogen diffusivities of 10^1 cm^2/year - 10^1 cm^2/ka
 398 (Figure 2B). A strong relationship between mineral structure and hydrogen diffusivity

399 is also seen (Figure 2C). Experiments by Kohlstedt and Mackwell (1998); Demouchy and
400 Mackwell (2006); Demouchy (2010) show a clear distinction between hydrogen diffusiv-
401 ity within crystalline aggregate and at grain boundaries (Figure 2D). For olivine, hydro-
402 gen diffusivity at grain boundaries is measured at $\sim 1 \text{ m}^2 \text{ year}^{-1}$, which can be consid-
403 ered instantaneous given an average grain boundary thickness of 0.75 nm (Demouchy,
404 2010).

405 Although such experimental results indicate that hydrogen diffusivity at grain bound-
406 aries and within mineral aggregates (e.g., fused quartz) can be significant, the effect is
407 outweighed by increasing grain size. Diffusivity decreases exponentially with increasing
408 grain size (Figure 2E). Grain sizes for crystalline rocks are a function of their cooling his-
409 tories, with cratonic crystalline basement and mantle xenoliths exhibiting average grain
410 sizes from millimetres to several centimeters. However, individual crystals can reach up
411 to 30 cm in size in some ultramafic mantle xenoliths with prolonged cooling histories (Hoskin
412 & Sundeen, 1985; Speciale et al., 2020; Sharapov et al., 2022)). Furthermore, the max-
413 imum temperatures of diffusivity experiments ($< 1600 \text{ K}$) are representative of man-
414 tle conditions and not encountered within the continental realm and sedimentary basins,
415 which typically vary between $\sim 300 - 500 \text{ K}$ (Hantschel & Kauerauf, 2009). The ex-
416 ponential relationship of Demouchy (2010) indicates a decrease in hydrogen diffusivity
417 of ~ 3 orders of magnitude between grain sizes of 10 mm and 0.1 mm, at which point
418 the relationship flatlines. Given these experiments were conducted at a pressure and tem-
419 perature representative of upper mantle conditions, it is reasonable to assume that the
420 diffusivity of olivine (and other minerals) at typical continental and sedimentary basin
421 conditions will be many orders of magnitude smaller than the measurements of Demouchy
422 (2010). Given these factors, experimental results indicate that native hydrogen entrained
423 within the mineral structure of crystalline rocks within the shallow Earth may diffuse
424 on geological timescales from the most common rock forming minerals. Geochemical data
425 obtained by Parnell and Blamey (2017) indicate that common felsic lithologies, such as
426 granites, gneiss and conglomerates of Archean - Proterozoic ($> 1600 \text{ Ma}$) age consis-
427 tently contain an order of magnitude greater hydrogen concentration in their entrained
428 fluid than very young ($< 200 \text{ Ma}$) granites. Parnell and Blamey (2017) found that sed-
429 imentary rocks containing clasts of old basement also included a greater proportion of
430 hydrogen than young granites and hypothesise that a signature of hydrogen in the base-
431 ment could be conferred to the sediment and that modern sediment derived from old and
432 young basement retains the signature of more or less hydrogen, respectively. It should
433 be noted, however, that the experimental results summarised by Parnell and Blamey (2017)
434 refer to bulk lithologies whereas those of Farver (2010) refer to individual minerals (e.g.
435 olivine and quartz). Furthermore, the preservation of high hydrogen abundances within
436 fluid inclusions and mineralised veins in ancient granites has been observed (Bourdet et
437 al., 2023). Hence, diffusion from enriched Archean - Proterozoic crystalline basement may
438 supply a ‘background’ hydrogen flux to overlying sedimentary basin rocks on geological
439 timescales. Hydrogen diffusion from coarse grained crystalline rocks, e.g. crystalline base-
440 ment, granites and their derived sedimentary products, e.g., conglomerates, must oper-
441 ate on timescales of Ma - Ga in order to explain the provenance of high hydrogen sig-
442 natures in sedimentary rocks that contain material sourced from enriched Archean - Pro-
443 terozoic basement. This is consistent with the widely documented observation of higher
444 hydrogen fluxes in sedimentary basins in continental cratonic regions underlain by Archean
445 - Proterozoic basement (e.g. Zgonnik (2020); Moretti, Brouilly, et al. (2021)). In the case
446 of rapidly cooled upper mantle rocks, e.g. MORBs, volcanic glasses, pillow lavas, how-
447 ever, grain sizes may be many orders of magnitude smaller than their continental coun-
448 terparts and within the nanometre scale (e.g., Schlinger et al. (1988)). Hence, hydrogen
449 diffusivity in rapidly cooled crystalline rocks and at MOR settings will be significantly
450 faster than in continental settings and potentially only a few orders of magnitude slower
451 than the lower temperature ranges of diffusivity experiments, i.e. 100 Ka - Ma or faster.
452 This is significant, since the age of most oceanic crustal rocks is $< 60 \text{ Ma}$ (Seton et al.,
453 2020), hydrogen diffusion within oceanic crustal rocks will operate on the same timescale

454 as the age of rocks themselves and provide a mechanism for the degassing of mantle hy-
 455 drogen to the surface and oceans.

456 *Diffusion in sedimentary rocks*

457 The rate of hydrogen diffusivity in sedimentary rocks is dependent on a wide range
 458 of factors, including lithology, porosity, permeability, temperature, pressure, salinity and
 459 water content. Typical values for hydrogen diffusivity in different sedimentary rocks, wa-
 460 ter and air are summarised in Table 2

461 Unlike for crystalline rocks and minerals, hydrogen diffusivity experiments for sed-
 462 imentary rocks are carried out at temperature and pressure conditions representative of
 463 sedimentary basins. These are typically at temperatures between 288–413 K and pres-
 464 sures < 40 MPa. A strong positive temperature dependence is seen in silt, clay, coal,
 465 shale and salt, whereby hydrogen diffusivity values vary by $> 50\%$ over a narrow range
 466 of ~ 40 K (C. Wang et al., 2024; J. Liu et al., 2022; Keshavarz et al., 2022; Vinsot et
 467 al., 2014). Hydrogen diffusivity decreases with increasing pressure, owing to increased
 468 fluid density at the same temperature and fixed space causing gas diffusion to be restrained
 469 (J. Liu et al., 2022). Measurements by J. Liu et al. (2022) of density profiles of hydro-
 470 gen in silt (montmorillonite) corresponding to different pressures indicate that the mineral
 471 adsorption layer is not influenced by increasing pressure, thus causing pressure to
 472 have an important but albeit lesser, effect on hydrogen diffusivity than temperature. At
 473 experimental conditions of 353 K and 10 MPa, a reduction in hydrogen diffusivity of \sim
 474 50% at a threshold water content of $\rho_{H_2O}^{ave} = 0.568$ gcm $^{-3}$, and $\sim 12\%$ as salinity in-
 475 creases from 8–12 wt% is observed in silt (J. Liu et al., 2022). This may be explained
 476 by the effects of increasing water content and salinity on the geometry of brine-rock and
 477 brine-hydrogen molecule contacts. When water content and salinity are low, hydrogen
 478 and brine form a stratified structure and the diffusivity of hydrogen is similar to that
 479 of confined pure gas at the same pressure and temperature conditions. Increasing wa-
 480 ter content and salinity leads to increased connectivity of brine molecules, the formation
 481 of water bridges between brine molecules and mixing of hydrogen and brine as a new phase,
 482 leading to a decrease in hydrogen diffusivity by up to 5 orders of magnitude (Figure 3,
 483 J. Liu et al. (2022)). Measurements of both dry and water-wet samples of various rock
 484 types by (Strauch et al., 2023) indicate that hydrogen diffusivity decreases further by
 485 an order of magnitude due to the effect of fracture healing with increased water content
 486 (Strauch et al., 2023). Hydrogen breakthrough times vary significantly with water con-
 487 tent, most notably for salt rocks whereby values increase from 1 – 843 hours.

488 Measurements of H $_2$ –brine contact angles versus pressure and total organic car-
 489 bon (TOC) in various water-wet Australian antracite shales by Al-Yaseri et al. (2022)
 490 indicate that capillary entry pressure decreases with increasing pressure and TOC, thus
 491 leading to a reduction in sealing capacity with depth and TOC. Within salt, hydrogen
 492 diffusion is strongly dependent on mineralogy, crystal shape and size. Diffusion through
 493 intact halite crystals with no discontinuities is negligible, whilst salt crystal boundaries
 494 and fractures within grains are the preferential flow paths for gas diffusion (Yuan et al.,
 495 2023).

496 Whilst hydrogen diffusivity experiments offer an insight into the absolute timescale
 497 of hydrogen migration through different materials, a more useful measure of sealing abil-
 498 ity is the breakthrough time. The breakthrough time, t_b is defined as the time interval
 499 between the start of gas purging of the feed chamber and the first detection of hydro-
 500 gen at the sensor in the permeate chamber. Whilst there are various methods to calcu-
 501 late t_b , the time-lag method of Frisch (1957) is widely applied due to its practicality and
 502 ability to allow for the transient definition of a microstructure dependent correlation of
 503 breakthrough time and sample thickness (Rhode et al., 2022). From Frisch (1957), $t_b \sim$

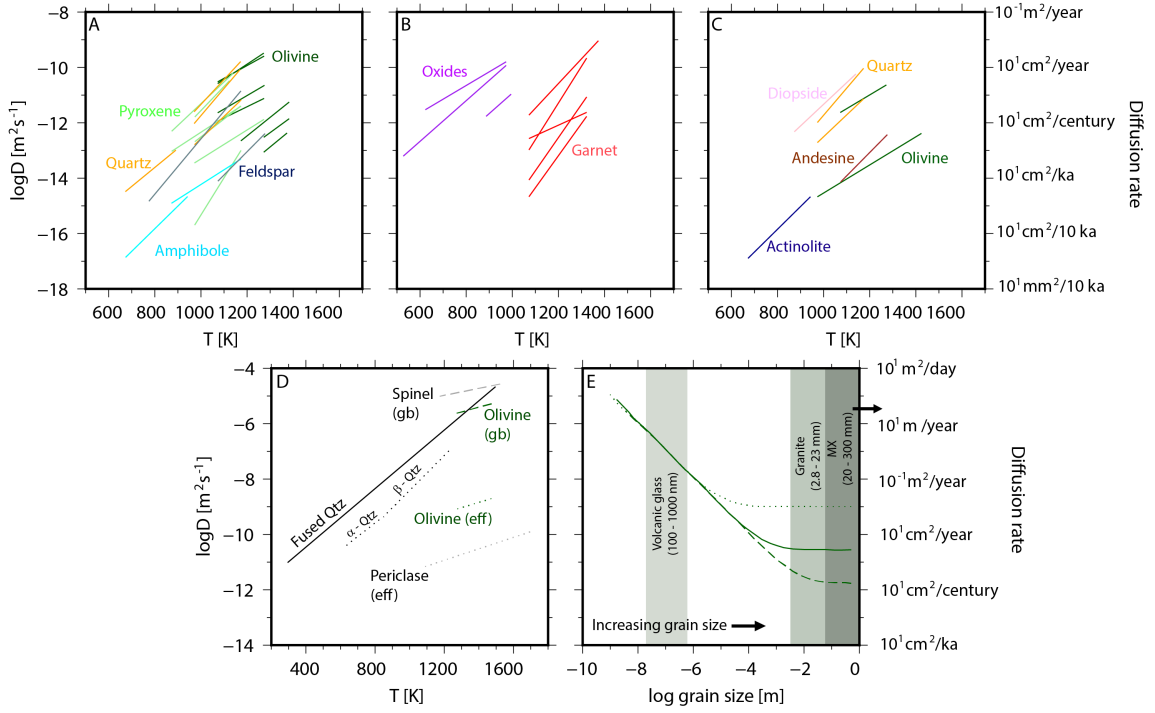


Figure 2. Hydrogen diffusivity as a function of mineralogy and lithology. A = Hydrogen diffusivity in the primary rock-forming minerals. These minerals constitute a significant component of Archean - Proterozoic crystalline basement (both mafic and felsic). B = Hydrogen diffusivity in oxides and garnets. C = Hydrogen diffusivity in different mineral structures. Whilst hydrogen diffusivity varies significantly with mineral structure, there is no obvious relationship between the two. D = Hydrogen diffusivity in fused, α and β quartz from (Li & Chou, 2015). Effective diffusivity in and diffusivity at grain boundaries (gb) for olivine, spinel and periclase from (Demouchy, 2010). Diffusivity at gb are several orders of magnitude greater than within crystal lattices. E = Hydrogen effective diffusivity in olivine aggregate at 1473 K and 300 MPa and grain boundary width = 0.75 nm (Demouchy, 2010). Hydrogen diffusivities are calculated using the gb diffusion from (Demouchy, 2010) and the “proton-vacancy” mechanism for lattice diffusion in olivine along [001] (dashed line) and along [100] and [010] (dotted line, Demouchy and Mackwell (2006) and “proton-polaron” mechanism for lattice diffusion in olivine along [100] (solid line, Kohlstedt and Mackwell (1998)). Diffusivity decreases exponentially with grain size. Grain size ranges for plutonic granites and mantle xenoliths (MX) are shown in medium and dark grey (Hoskin & Sundeen, 1985; Speciale et al., 2020). Black horizontal arrow indicates MX grain sizes beyond the axes range (e.g., Sharapov et al. (2022)). Typical grain sizes for microcrystalline volcanic glasses vary from 100 – 1000 nm and are shown in light grey (Schlinger et al., 1988). Diffusivity data from Farver (2010) (A-C), citetDemouchy2010, Li2015 (D-E). Panel E modified from Demouchy (2010).

Rock type	Diffusivity [m^2s^{-1}]	t_{b_1} (dry) [years]	t_{b_1} (wet) [years]	Reference
Bentheimer sandstone	$1.6 - 2.1 \times 10^{-9}$	2.5	3.3	Strauch et al. (2023)
Silt (montmorillonite)	$4.25 - 8.27 \times 10^{-8}$	0.06	0.12	(J. Liu et al., 2022)
Opalinus Clay	$1.2 - 5.13 \times 10^{-9}$	1.0	4.4	Vinsot et al. (2014)
Coal (anthracite)	$1.3 - 7 \times 10^{-8}$	0.08*	0.52*	Strauch et al. (2023)
Shale	$1.3 - 2.4 \times 10^{-8}$	2.2	3.7	Bagreev et al. (2004), Keshavarz et al. (2022)
Werra rock salt (halite)	$1.4 \times 10^{-9} - 1.3 \times 10^{-8}$	0.40	3.7	Al-Yaseri et al. (2022)
Water (pure)	$3.9 - 6.1 \times 10^{-9}$			Strauch et al. (2023)
Air	$0.756 - 1.604 \times 10^{-4}$	0.3 hours	0.6 hours	de Blok et al. (1982)
Stainless steel	1.5×10^{-11}	352		Ferrell and Himmelblau (1967)

Table 2. Hydrogen diffusivity values for various sedimentary rock types and materials and breakthrough times through 1 m of material, t_{b_1} , estimated using the time-lag method (see body text). Hydrogen diffusivity experiments for sedimentary rocks are conducted at temperatures and pressures representative of sedimentary basin conditions and are much lower than experimental conditions used for crystalline rocks and minerals. Variation in diffusivity values are due to dry and wet samples. The temperatures and pressures applied to the experimental results summarised in this table vary between 288 – 413 K and < 40 MPa, respectively. The diffusivity of hydrogen in pure water, air and stainless steel are included for reference. *Due to lack of available data in the literature, values for coal are estimated using H_2S diffusivity measurements (Bagreev et al., 2004).

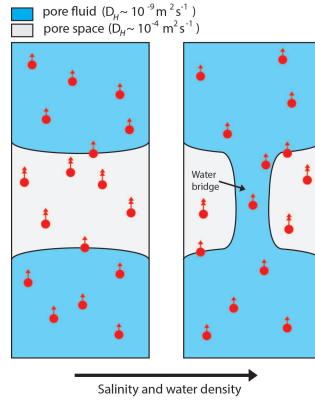


Figure 3. Effects of increasing salinity and water density on hydrogen diffusivity. Increasing salinity and density of pore fluid within sedimentary rocks leads to the formation of water bridges and increased connectivity between brine molecules, inhibiting the diffusion of hydrogen. Red circles = hydrogen molecules. Diffusion rates of hydrogen (D_H) in air are up to five orders of magnitude greater than in water and are indicated by double and single arrows, respectively. Modified from (J. Liu et al., 2022)

504 $L^2/6D_H$, whereby L = length of sample thickness. Hence, the breakthrough time through
 505 1 m of rock may be approximated as $t_{b1} \sim 1/6D_H$.

506 Using published values, estimated t_{b1} values for sedimentary rocks are shown in Ta-
 507 ble 2. t_{b1} values are on the scale of years for dry and wetted rock samples, with break-
 508 through times for wetted rocks typically several times greater than for dry rocks (Strauch
 509 et al., 2023; J. Liu et al., 2022; Vinsot et al., 2014; Keshavarz et al., 2022; C. Wang et
 510 al., 2024; Al-Yaseri et al., 2022; de Blok et al., 1982; Ferrell & Himmelblau, 1967; Jacops
 511 et al., 2017; Hemme & van Berk, 2018; Mostinsky, 2011; ToolBox, 2018; Owczarek & Za-
 512 kroczymski, 2000).

513 **Advection**

514 Advection is the transport of a substance due to the motion of a carrier, e.g. wa-
 515 ter. In the case of hydrogen, gaseous H_2 may also be carrier for itself. Advective trans-
 516 port systems within the subsurface include fluid migration along faults and discontinu-
 517 ities and groundwater flow through aquifers. By its nature, the advection of hydrogen
 518 through sedimentary basins is a complex process that cannot be described in a single step.
 519 A hydrogen molecule may migrate from depth to the surface through a combination of
 520 advection and diffusion during its ascent.

521 ***Migration in porous media***

522 Migration through porous sedimentary rocks is one of the most significant mech-
 523 anisms of fluid transport within sedimentary basins across the world. Fluids, such as hy-
 524 drocarbons and CO_2 , displace and interact with formation fluids present within the pore
 525 spaces in sedimentary rocks, with flow directed along pressure gradients exerted on the
 526 system. In the case of hydrogen, transport via dissolution in groundwater within aquifers
 527 is one of the primary mechanisms of advective migration in the shallow Earth. Natural
 528 hydrogen migration via transport within sedimentary rocks and groundwater has not re-
 529 ceived much attention in literature and is not yet well understood. It is however known

530 to be affected by factors such as salinity, temperature, pressure, formation fluid compo-
531 sition and fluid-rock interactions.

532 Shallow aquifers have typical depths from near-surface to ~ 100 m, whilst deep
533 aquifers may reach up to 9000 m. Temperature and salinity ranges in aquifers vary be-
534 tween $7 - 174^\circ\text{C}$ and $5 - 52000$ ppm, respectively (Dopffel et al., 2021). These factors
535 exert a primary control on both the solubility of hydrogen in groundwater and micro-
536 bial abundance and activity, which have important implications for hydrogen migration
537 (e.g. Berta et al. (2018); Koproch et al. (2019)). Similar to other gases, the solubility
538 of hydrogen in water decreases proportionally with salt (NaCl) concentration, until the
539 solution is saturated (Chabab et al., 2020). Recent solubility data of hydrogen in water-
540 brine under geological conditions typical of aquifers were used by Chabab et al. (2020)
541 to determine empirical relationships between hydrogen solubility and salt concentration
542 in pure water and brine with 0.5–2% Average Absolute Deviation to observed values.
543 These are:

$$x_{H_2}^0 = b_1PT + \frac{b_2P}{T} + b_3P + b_4P^2 \quad (1)$$

544 for pure water at $273.15 < T < 323.15$ K and $0.1 < P < 20.3$ MPa, and

$$\ln\left(\frac{x_{H_2}}{x_{H_2}^0}\right) = a_1m_{NaCl}^2 + a_2m_{NaCl} \quad (2)$$

545 for brine at $323.15 < T < 373.15$ K, $P_1 < P < 23$ MPa and $m_{NaCl} < 5$ mol/kg,
546 whereby T = temperature, P = pressure, X_{H_2} = hydrogen solubility, $x_{H_2}^0$ = hydro-
547 gen solubility in pure water, m_{NaCl} = molality of salt and a_i, b_i = empirical coefficients
548 listed in (Chabab et al., 2020). The amount of dissolved hydrogen decreases with increas-
549 ing salinity (see Figure 9 Chabab et al. (2020)). New measurements of hydrogen solu-
550 bility carried out under conditions of high pressure (< 20 MPa), temperatures ranging
551 from 298–373 K and salinities < 4 mol/kgw of NaCl by Chabab et al. (2024) indicate
552 that H_2 solubility in water and brine increases with pressure and follows Henry’s law in
553 a quasi-linear trend. Models optimised on experimental data predict a minimum solu-
554 bility temperature ($T_{xH_2,min}$) of around ~ 326 K in pure water, decreasing with salin-
555 ity ($T_{xH_2,min} = 315\text{K}$ at 2 molal NaCl and $T_{xH_2,min} = 288\text{K}$ at 4 molal NaCl) (Chabab
556 et al., 2024).

557 The interaction between natural hydrogen and resident formation fluid, e.g. wa-
558 ter, present within the pore spaces of sedimentary rocks is also of significance as this in-
559 fluences the displacement of the former over the latter within geological porous media.
560 Measurements of hydrogen-brine interfacial tension, γ , over a wide range of T, P and
561 m_{NaCl} ranges by Hosseini et al. (2022) indicate an inverse linear relationship between
562 γ, P and T . γ was found to have a strong dependence on temperature, and decreased
563 linearly at constant pressures and salinity. γ increased significantly and linearly with in-
564 creasing salinity at constant temperatures and pressures, whilst decreasing at a lower rate
565 with increasing pressure at constant temperature and salinity due to the increasing inter-
566 molecular forces between hydrogen and water at elevated pressures (Iglauer et al., 2012;
567 Hosseini et al., 2022). Hence, temperature and salinity have a greater effect than pres-
568 sure on the solubility of hydrogen and its ability to displace formation fluids within porous
569 media (Hosseini et al., 2022; J. Liu et al., 2022). With regards to diffusivity, simulations
570 of molecular dynamics at subsurface conditions conducted by Kalati et al. (2024) indi-
571 cate lower diffusivity at higher salinity and lower temperature, the value being $7.29 \times$
572 10^{-9} m^2/s at 323 K, increasing to 10.2×10^{-9} m^2/s at 353 K for 1 molal NaCl solu-
573 tion. The diffusion coefficient decreases up to 38% as the salinity increases from 1 to 5
574 molal (Kalati et al., 2024). The results of Kalati et al. (2024) correspond to simulation

575 results by Lopez-Lazaro et al. (2019), which measure the temperature minimum hydro-
 576 gen solubility close to 326 K.

577 *Migration along faults and fractures*

578 The episodic circulation of fluids and gases along geological faults is intricately con-
 579 trolled by mechanisms governing fault opening and sealing, as well as the timing of these
 580 processes. Fluid advection along crustal faults is a well-documented phenomenon (Cox
 581 & Etheridge, 1989), and it is a recurrent occurrence in the Earth’s crust (Marques et al.,
 582 2018). These faults play a pivotal role in the migration of gas such as hydrogen, serv-
 583 ing as both conduits and barriers. Studies at both reservoir and basin scales have demon-
 584 strated that fault transmissivity is primarily influenced by (i) the fault’s type, geome-
 585 try, and displacement; (ii) the internal architecture of the fault zone; (iii) the surround-
 586 ing stratigraphy and lithology; and (iv) the geomechanical stress (Faulkner et al., 2010;
 587 Solum et al., 2010; Massiot et al., 2019). Due to the variability of these parameters, fault
 588 transmissivity evolves both temporally and spatially (Frery et al., 2015; Frery, Fryer, et
 589 al., 2021). The opening of faults can be triggered by seismic events, fluid overpressures,
 590 or localised dissolution (Gratier & Gueydan, 2007), while their closure can be attributed
 591 to progressive sealing resulting from mechanical (Hancock et al., 1999; Eichhubl & Boles,
 592 2000), chemical processes and fault roughness (Renard et al., 2013).

593 Fault zones are complex features that can be effectively modelled as damaged zones
 594 and gouges with heterogeneous porosity and permeability architectures. For instance,
 595 in the North Perth Basin (Australia), these fault zones exhibit a highly compartmen-
 596 talised nature, primarily acting as barriers to crossflow while driving upward fluid mi-
 597 gration. This structural configuration provides an ideal setting for structurally controlled
 598 hydrogen migration (Frery, Langhi, et al., 2021). For instance, above a natural subsur-
 599 face CO₂ reservoir, a causal relationship between CO₂ pulsing and fault opening have
 600 been demonstrated using isotopic analysis (C, O, Sr ratios, Ba/Ca, and Sr/Ca elemen-
 601 tal ratios)(Kampman et al., 2012). The opening of veins is associated with a pulse of CO₂
 602 within the system, followed by a degassing phase that occurs simultaneously with vein
 603 growth. Consequently, abrupt events may have triggered the opening of fractures, im-
 604 mediately followed by episodes of fluid circulation. Evidence of fault opening events can
 605 be observed with durations ranging from millennia to centuries (Burnside et al., 2013;
 606 Frery et al., 2015; Gratier & Gueydan, 2007).

607 In regions of active faulting, stress cycling and the creation and destruction of per-
 608 meability and fluid flow are closely linked . Both large (km) and small-scale (j m) faults
 609 are capable of influencing fluid migration pathways within sedimentary basins. The ad-
 610 vection of hydrogen-enriched fluids along large-scale faults are attributed to natural hy-
 611 drogen fluxes recorded in several well-known case studies, including Mali, Brazil and the
 612 north Pyrenees (France) (Prinzhofer et al., 2018; Myagkiy, Brunet, et al., 2020; Donzé
 613 et al., 2020; Lefeuvre et al., 2022). Common factors include the intersection of deep, crustal-
 614 scale faults with Archean-Proterozoic crystalline basement or ultramafic mantle bodies
 615 that are serpentinised, hydraulic or elevated temperature and pressure gradients that trig-
 616 ger fluid migration. Measured daily flow rates of gaseous H₂ flux within fault zones by
 617 Lefeuvre et al. (2022) ranges from 0.07–0.15 m³m⁻²d⁻¹ in the north Pyrenees. These
 618 values are comparable to measurements of gaseous H₂ flux within soils from the Sao Fran-
 619 cisco basin in Brazil and the Semail ophiolite, Oman (Prinzhofer et al., 2019; Zgonnik,
 620 2020; Moretti, Prinzhofer, et al., 2021). The measurements of Lefeuvre et al. (2022) equate
 621 to a timescale of ~ 128 – 274 years for hydrogen migration over a distance of ~ 7 km
 622 from its serpentinite source to trap beneath a clay-rich seal. Templeton et al. (2024) note
 623 that whilst low temperature water-rock reactions produces net H₂ from the oxidation
 624 of Fe(II)-bearing minerals within the Semail Ophiolite, biological activity is predicted
 625 to be stimulated by fluxes of H₂, giving rise to net H₂ consumption. The most proba-
 626 ble detection of H₂ at the surface is at hyperalkaline seeps sourced by deep faults, rather

627 than in most soils and peridotite outcrops, due to efficient microbial H_2 scavenging of
 628 the available H_2 flux in the upper aquifer, where measured $H_2(aq)$ levels drop below de-
 629 tection (Templeton et al., 2024). Hence, from a migration perspective it is reasonable
 630 to hypothesise that the migration of hydrogen-rich fluids along faults within the upper
 631 several kilometers of the subsurface in this instance must occur over a timescale of hours
 632 to days, and must be faster the timescales of biogenic reactions responsible for hydro-
 633 gen consumption.

634 Aside from large-scale faulting, complex networks of small-scale (10–100 m throw)
 635 faults restricted to individual sedimentary layers, known as polygonal fault systems (PFS)
 636 have been identified as having important impacts on basin-scale fluid flow. The impact
 637 of PFS on fluid migration is debated within the literature, with authors attributing PFS
 638 for both enhancing (e.g., Ireland et al. (2021); Cartwright (2011); Cartwright et al. (2003))
 639 and restricting (e.g., Xia et al. (2022); Andresen and Huuse (2011)) fluid flow. Whilst
 640 PFS have been identified as a mechanism for seal bypass (Ireland et al., 2021), perme-
 641 ability may be effectively destroyed by clay smearing along fault planes and thus increase
 642 the sealing capacity of PFS (Xia et al., 2022; Andresen & Huuse, 2011). Basin inversion,
 643 fault reactivation or dewatering of host sediments may lead to the periodic opening of
 644 fluid, and thus hydrogen migration pathways along impermeable PFS (Xia et al., 2022).
 645 Whilst PFS must inevitably enhance the passage of fluids during their diagenesis, it is
 646 unlikely that PFS and microfractures provide substantial hydrogen migration pathways
 647 over geological timescales during periods of tectonic quiescence. However, PFS may be
 648 capable of both providing a mechanism for fluid communication and opening hydrogen
 649 migration pathways on short geological timescales during periods of tectonic activity or
 650 fault slip.

651 Whilst faulting and fluid flow have been extensively reviewed in the literature, their
 652 impact on hydrogen migration have only recently gained significant attention. Early work
 653 by Wakita et al. (1980) hypothesised the production of hydrogen by fault movement,
 654 based on measurements of elevated hydrogen concentrations ($> 3\%$ by volume) around
 655 active fault zones in southwestern Japan compared to background measurements of \sim
 656 0.5 ppm. Su et al. (1992) identified the potential reduction in strength of crystalline min-
 657 erals (e.g., calcite, dolomite, antigorite) due to hydrogen infiltration at low pressures, lead-
 658 ing to the weakening of rocks and initiation of faulting. Hydrogen gas measurements and
 659 particle size distribution analyses by Niwa et al. (2011) within an active fault zone in-
 660 dicate that hydrogen gas mostly migrated in permeable fracture zones by advection with
 661 groundwater. Firstov and Shirokov (2005) measured seven pulses of hydrogen discharge
 662 against background levels in a fault zone trending parallel the Kuril - Kamchatka geostruc-
 663 tural zone, Russia, from 1999–2003. Hydrogen pulses preceding seismic events lasted
 664 from 1.5–6 hours and were 2–14 times higher than measured background levels. Firstov
 665 and Shirokov (2005) found that $< 80\%$ earthquakes with $M_W \geq 5.6$ in the southern
 666 Kamchatka region occurred within one month of measured hydrogen pulses and consid-
 667 ered such events as short-term earthquake precursors. In recent years, the migration of
 668 natural hydrogen from deep crustal sources along kilometre-scale faults which penetrate
 669 crystalline basement have been recorded in several locations across the world (e.g., Brazil,
 670 France, Mali) (Prinzhofer et al., 2018; Deronzier & Gouze, 2020; Donzé et al., 2020; Rezaee,
 671 2021; Frery, Langhi, et al., 2021; Lefevre et al., 2021, 2022).

672 *Surface seeps*

673 Surface hydrogen emissions are associated with a wide range of geological condi-
 674 tions, including serpentinised mafic rocks, rift zones, Precambrian rocks, volcanic rocks,
 675 volcanic gases, geysers, hot springs, mud volcanoes and isolated seeps. The emission of
 676 natural hydrogen and gas from surface seeps has been recognised for millennia, e.g., the
 677 continuously burning Olympic flame at Mount Olympus, Turkey, dating back 2500 years
 678 and comprised of 7.5–11.3% H_2 (Hosgörmez, 2007). Other examples include ‘Los Fue-

Type	Example	Characteristics	Reference
H ₂ -rich	‘Los Fuegos Eternos’, Philippines	Noble gas signatures similar to air, pH < 10	Vacquand et al. (2018) Abrajano et al. (1990)
N ₂ -rich	Semail, Oman	Ophiolitic, ³ He/ ⁴ He < 1R _A	Sano et al. (1993)
N ₂ -H ₂ -CH ₄	New Caledonia	Ophiolitic, mixing of CH ₄ -H ₂ and N ₂ -rich components	Deville and Prinzhofer (2016)
H ₂ -CH ₄	Mount Olympus, Turkey Zambales, Philippines	Ophiolitic, active subduction, ³ He/ ⁴ He > 1R _A	Abrajano et al. (1988) Hosgörmez (2007)

Table 3. Characteristics of surface abiogenic hydrogen seeps compiled from various references.

679 gos Eternos’ (the eternal flames), discovered in the Philipines over two centuries ago with
680 H₂ concentrations of 41.4–44.5% (Vacquand et al., 2018; Abrajano et al., 1990). The
681 distribution of surface hydrogen seeps across the globe are reviewed extensively by Zgonnik
682 (2020), and can be separated into four broad categories (Table 3).

683 A common characteristic of most abiogenic natural hydrogen seeps is an associa-
684 tion with ultramafic rocks, ophiolites and serpentinisation. The hydrolysis and oxida-
685 tion of primary ferromagnesian minerals, such as olivine and pyroxenes, produces H₂ over
686 a wide range of environmental conditions (Holm et al., 2015). Elevated isotopic signa-
687 tures, i.e. ³He/⁴He < 1R_A, within hydrogen-rich fluids encountered at such surface seeps
688 owe their provenance to primordial or deep mantle enrichment within ultramafic hydro-
689 gen source rocks. However, whilst the advection of hydrogen entrained within ultramafic
690 rocks occurs over undoubtedly geological timescales, its liberation and transport to the
691 surface must depend on the parameters driving the H₂-forming serpentinisation reac-
692 tion. Measurement of H₂ degassing using in-situ gas chromatography and analysis of ex-
693 perimental products using XRD, Raman and X-ray absorption spectroscopy under ser-
694 pentinisation conditions (300°C and 30 MPa) show a three stage process during the ser-
695 pentinisation reaction: early (0 – 18 days), intermediate (18 – 34 days) and late (34 –
696 70 days). At the earliest stage, hydrogen is generated due to the crystallisation of mag-
697 netite, with Fe-rich serpentine also formed as a reaction product of olivine, enstatite, clinopy-
698 roxene and water. As the reaction progresses during the intermediate phase, hydrogen
699 is generated due to the formation of serpentine and clinopyroxene is absent from the re-
700 action. During the final stages of serpentinisation, the serpentinisation front has effec-
701 tively disappeared and hydrogen is generated due to the oxidation of Fe-rich serpentine
702 (Figure 4A, Table 4, Marcaillou et al. (2011)). The results of Marcaillou et al. (2011)
703 are further supported by Greenberger et al. (2015), who investigated the progression of
704 serpentinisation by mapping Fe oxidation states and analysing stable isotopes of carbon
705 and oxygen in carbonates to constrain the conditions of water–rock interaction during
706 serpentinisation. As groundwater migrates through a rock volume, the area of contact
707 between ultramafic source rocks (e.g., harzburgite, olivine) and migrating fluids, i.e. ser-
708 pentinisation front, is greatest at early stages of serpentinisation. The serpentinisation
709 front is reduced as the reaction progresses, with maximum H₂ generation at the earli-
710 est stages of serpentinisation (Figure 5B Greenberger et al. (2015)).

711 Within subduction-related and ophiolitic terrains, all four types of seeps listed on
712 Table 3 are encountered. However, the nature of gases and gaseous mixtures emitted at
713 surface seeps is dependant on geodynamic context and the proportionality of mixing be-
714 tween different fluids. Noble gases display signatures close to the value of air in H₂-rich
715 seeps, indicating that hydrogen gas emitted from ophiolitic settings is generated at shal-
716 low depths within Earth’s crust. N₂-rich seeps are notably associated with relatively high
717 contents of crustal ⁴He, and the source of N₂ is interpreted as derived mainly from meta-
718 morphosed sediments located on the subducted crustal slab, below the ophiolitic units

Stage	Reaction	Reaction time
Early	Olivine + enstatite + cpx + H ₂ O + H ⁺ → Serpentine + magnetite + Mg ²⁺ + Ca ²⁺ + SiO ₂ + H ₂	0 – 18 days
Intermediate	Olivine + enstatite + H ₂ O + SiO ₂ + Mg ²⁺ → Serpentine + magnetite + H ⁺ + H ₂	18 – 34 days
Late	Enstatite + cpx + Fe-rich serpentine + H ₂ O → Mg-rich serpentine + magnetite + calcic silicate + H ₂	34 – 70 days

Table 4. Stages of the serpentinisation reaction (Marcaillou et al., 2011)

(Deville & Prinzhofer, 2016; Vacquand et al., 2018). H₂–CH₄-rich gas seeps are typically characterised by mantle-like C and noble gas characteristics, as evidenced by measurements from several locations including the Zambales ophiolite, Phillipines and New Caledonia. Fluid communication within fracture networks and mixing between N₂-rich H₂–CH₄-rich end members is the most likely cause for N₂–H₂–CH₄-rich gas seeps (Abrajano et al., 1990; Deville & Prinzhofer, 2016). The flux of deep gas into a shallow aquifer isolated from direct equilibrium with the atmosphere and fractionation during subsequent degassing is suggested by Deville and Prinzhofer (2016) as the simplest explanation for observed ²⁰Ne and ³⁶Ar concentrations. A schematic diagram of the distribution of different gas seeps with an ophiolitic terrain is shown Figure 5A.

The timescale of subsurface gas migration is also dependent on parameters that control groundwater transport properties. Experimental work by Lamadrid et al. (2017) used synthetic fluid inclusions as micro-reactors in olivine crystals to monitor serpentinisation rates in-situ and at serpentinisation conditions (280°C). Serpentinisation rates were strongly influenced by aqueous fluid salinity, with evidence of reaction after 5 days decreasing from 50% to zero as aqueous fluid salinity of synthetic inclusions increased from 1–10 wt%. The time taken to observe the first evidence of reaction for salinity experiments at 10 wt% was 120 days, with the average rate of reaction being two orders of magnitude lower than experiments conducted with 1 – 3.5 wt% salinity (Lamadrid et al., 2017). The results of Lamadrid et al. (2017) support those of Rouméjon and Cannat (2014), and indicate that the forward reaction requires continual influx of a lower salinity aqueous fluid (seawater) to dilute the serpentinisation fluid and allow serpentinisation of olivine to continue. Hydrogen migration and emission from surface seeps is dependent on the interplay between generative processes (e.g. serpentinisation) and destructive processes (e.g. microbial consumption). Important factors which influence the balance between generation and consumption include the water/rock ratio of migration or injected fluids (e.g. stimulated hydrogen generation, see next section), fluid chemistry and the formation of Fe(III)-bearing secondary phases (Templeton et al., 2024).

The results of Lamadrid et al. (2017) and Rouméjon and Cannat (2014) complement experimental results of hydrogen dissolution by Iglauer et al. (2012) and Hosseini et al. (2022) (see earlier sections), and lead to an overall consensus that the salinity of the carrier fluid (i.e., groundwater) is a major controlling factor in both the amount of hydrogen gas generated and its rate of transport within sedimentary basins and ophiolitic terranes.

Stimulated hydrogen generation

Over the last few years, the concept of stimulated geological hydrogen, also known as ‘orange’ hydrogen, has gained significant momentum (e.g., Osselin et al. (2022); Templeton et al. (2024)). Hydrogen generation may be stimulated by the injection fluids into target rock formations rich in reactive Fe(II)-bearing minerals to promote the overar-

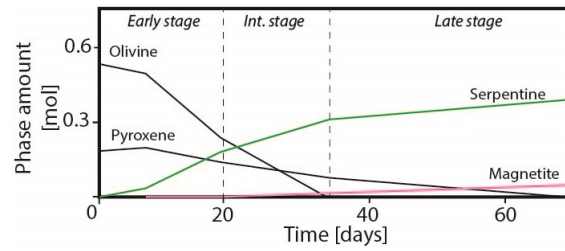


Figure 4. Evolution of mineral phases during serpentinisation reactions shown on Table 4. Serpentinisation products are shown in red (serpentinite) and red (magnetite). Magnetite crystallises first and is responsible for H₂ generation during the early stage. During the intermediate phase, clinopyroxene is absent due to a lack of enrichment of calcium. During the late stage, olivine is no longer the reactive species and is replaced by serpentine formed during the early phase as the reactant. Late stage serpentine is Mg-rich and distinct from early stage serpentine. Modified from (Marcaillou et al., 2011).

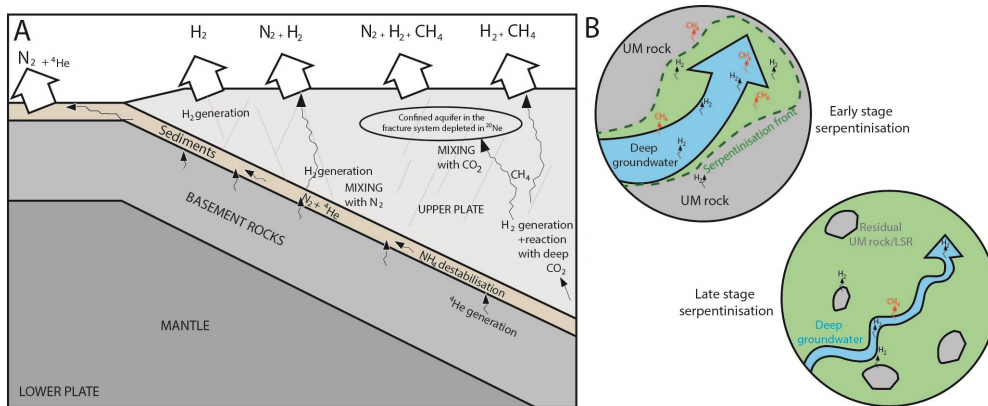


Figure 5. A = Conceptual diagram explaining gas compositions found at ophiolite-related seeps. B = Conceptual diagram showing progression of serpentinisation reaction and fluid migration pathways. UM rock = ultramafic rock. As serpentinisation of a rock volume progresses, water/rock ratios decrease significantly due to volume expansion and reduced permeability of serpentine (O’hanley, 1992). During late stage serpentinisation, H₂ generation decreases significantly due to reduced contact between serpentinisation fluids (e.g. deep groundwater) and reactants (unreacted ultramafic rock and early stage Fe-rich serpentine). Modified from (Marcaillou et al., 2011; Greenberger et al., 2015; Deville & Prinzhofer, 2016; Vacquand et al., 2018).

ching reaction of $2\text{FeO}(\text{rock}) + \text{H}_2\text{O} \rightarrow \text{Fe}_2\text{O}_3(\text{rock}) + \text{H}_2$. Most commonly, these are found within ultramafic rocks or ophiolites. H_2 is then extracted by recirculating injected fluids to the surface, if the required (bio) geochemical conditions for rapid hydrogen production have been met (Templeton et al., 2024). Development of this relatively new concept has been spurred by the recent U.S Department of Energy announcement of funding to support research into the production of geologic hydrogen through stimulated mineralogical processes (of Energy, 2024).

However, it is worth noting that the term ‘orange’ hydrogen has a broader meaning within the literature, and includes chemical processes that break down traditional hydrocarbons and biofuels (e.g., crude oil, natural gas, gasoline, biogas, etc.) into hydrogen with no carbon dioxide byproduct (Neelameggham et al., 2022). A notable recent study that explores this includes the generation of H_2 from H_2S by thermal splitting, a process which is potentially $\sim 38\%$ more economically viable than green hydrogen production (Nova et al., 2023). As this review is focussed on subsurface hydrogen and migration, we do not explore industrial and chemical processes capable of producing hydrogen and avoid the term ‘orange’ hydrogen to prevent confusion with stimulated hydrogen generation, i.e. due to the injection of fluids within subsurface geological formations.

Osselin et al. (2022) assessed the reactive percolation of a NaHCO_3 -rich brine at 160°C and 280°C in natural serpentinite cores in order to study the dynamic competition between serpentinisation and carbonation of ultramafic formations. Their results are used to suggest that up to 100 trillion tonnes of H_2 could be produced from Fe(II)-bearing rocks near Earth’s surface. Similar to the serpentinisation reactions shown on Table 3, the experiments of Osselin et al. (2022) were completed over a time period of days. However, it is important to note that permeability reductions of several orders of magnitude were observed and attributed to the precipitation of carbonates in the main percolation paths. In mafic rocks, permeability is produced by fractures and the reduction in fracture permeability with time can be approximated by an exponential function: $k_f = k_{f0}e^{-t/t^*}$, where k_{f0} is the starting permeability of the modelled interval and t^* is the characteristic decay time of the best fit exponential function in hours (Farough et al., 2016). Precipitation of carbonates over silicates is favoured due to fast reaction kinetics in comparison to flow rates. Osselin et al. (2022) conclude that the spatio-temporal lengthscales associated with the different chemical reactions are directly linked to the ratio of chemical reaction rate and transport (also known as the Damkohler number) and to the type of reaction regime (transport-limited vs reaction-limited). They interpret their results as a dynamic interplay between dissolution and precipitation, controlled by the local flow rate and the local pore geometry. Osselin et al. (2022) note that the complex pore size distribution in natural rocks leads to very different behavior even for a homogeneous mineralogy. Hence, the work of Osselin et al. (2022) demonstrates the significance of changes in material properties of host rocks due to the flow of fluids used to liberate hydrogen from mafic minerals, which will occur on a timescale of days.

More recently, Templeton et al. (2024) discusses factors that influence the timescales of fluid migration through the Semail Ophiolite, Oman, such as the hydraulic conductivity of partially-hydrated peridotites, the extent of fracturing, and the geochemical dynamics of the subsurface environment. Fluid flow in the most shallow and fissured rocks occurs in transmissive zones located within 50 m of the surface, indicating that fluid dynamics are highly heterogeneous. Templeton et al. (2024) also describes that some zones are most sensitive to conductive channels, such as partially mineralised fractures, whereas other zones are supplied from rocks above and below. This complexity, including the presence of fractures partially filled with secondary minerals produced from both modern and ancient water/rock reactions, suggests that fluid migration rates and, by extension, hydrogen migration rates through the crust are highly variable and dependent on local geological conditions. In contrast to Osselin et al. (2022), the analyses of Templeton et al.

811 (2024) were conducted at low temperature (25°C), demonstrating that the sensitivity
 812 of fluid flowpaths are not restricted to high-temperature systems only or within deeper
 813 parts of geological basins.

814 **Adsorption**

815 The migration of hydrogen may be prevented by the physical adsorption of H₂ molecules
 816 to the surface of minerals, particularly clays. This is demonstrated by Truche et al. (2018),
 817 who demonstrate hydrogen enrichment of < 500 ppm (0.25 mol/kg of rock) within organic-
 818 poor (< 0.5 wt % total organic carbon) clays composed of illite, chlorite and kaolinite
 819 from the Cigar Lake uranium ore deposit, Canada. Furthermore, recent experiments by
 820 L. Wang, Cheng, et al. (2023) demonstrate that hydrogen adsorption is significantly in-
 821 fluenced by the pore structure and specific surface area of the clay minerals, with a no-
 822 table increase in hydrogen adsorption capacity under high pressure and a decrease at higher
 823 temperatures, independent of the clay mineral type. L. Wang, Cheng, et al. (2023) show
 824 that whilst montmorillonite and chlorite only adsorb hydrogen on their external surface,
 825 palygorskite and sepiolite can adsorb hydrogen on both the bulk phase and the exter-
 826 nal surface. However, adsorption capacity may be compromised by a range of factors,
 827 including the presence of water and other adsorbed gases (e.g., CO₂, CH₄, He) which
 828 may compete for adsorption sites.

829 Whilst significant volumes of hydrogen may accumulate within clay-rich rocks due
 830 to adsorption, the degree to which this affects overall hydrogen migration on the basin-
 831 scale is, however, an open question. Truche et al. (2018) estimate that 4 – 17% of H₂
 832 produced by water radiolysis over the 1.4 Ga lifetime of the Cigar Lake uranium ore de-
 833 posit is trapped in the surrounding clay alteration halos, thus leaving 83–96% hydro-
 834 gen unaccounted for. Despite adsorption, hydrogen will migrate due to advection along
 835 fractures and by diffusion, with breakthrough times varying on the scale of years per me-
 836 tre for most rocks, including clays (Table 2). Hence, it is reasonable to assume the timescale
 837 over which adsorption sites become occupied must be fairly rapid and on the scale of years
 838 to thousands of years for volumes of clay-rich rocks typically within sedimentary basins.
 839 In reality, it is likely that whilst adsorption may trap significant and potentially economic
 840 volumes of hydrogen within clay-rich rocks and remain stable over geological timescales,
 841 the majority of hydrogen within sedimentary basins remains transient and mobile.

842 **Microbes**

843 Microbial reactions within host rocks and sediments are important moderators of
 844 hydrogen flow in the subsurface. Microbial activity may lead to both the generation and
 845 loss of hydrogen as it migrates through a reservoir, as summarised on Table 5. Micro-
 846 bial reactions are dependent on many factors, such as environment (e.g., pH, salinity),
 847 iron (Fe³⁺) content of host rocks, groundwater recharge and the presence of other re-
 848 duced gases from deeper in Earth (Anderson et al., 1998; Stevens & McKinley, 2000).
 849 There is a growing consensus that subsurface microbial communities are independent of
 850 photosynthesis for carbon and hydrogen supply, and are primarily or completely depen-
 851 dent on abiotic hydrogen sources in various geological settings as an energy source (Kotelnikova
 852 & Pedersen, 1998; Takai et al., 2004; L. H. Lin et al., 2005; McCollom & Amend, 2005;
 853 Nealson et al., 2005; Escudero et al., 2018; Gregory et al., 2019). These microorganisms
 854 consist of Bacteria and Archaea and exist in great abundances within the subsurface, with
 855 $\sim 10^4 - 10^8$ cells/gram of rock up to several km deep and $\sim 2 - 6 \times 10^{29}$ cells within
 856 the continental subsurface (Dutta et al., 2018; Magnabosco et al., 2018). For microbial
 857 life to survive, temperature limits must lie between -15°C to $+121^\circ\text{C}$, corresponding
 858 to depths of up to 3.5 – 4.5 km beneath Earth’s surface at normal geothermal gradi-
 859 ents of $30 \pm 5^\circ\text{C}/\text{km}$. Temperature, pressure and salinity are important factors for the
 860 prevalence of single-celled microorganisms within the subsurface that are responsible for
 861 using hydrogen in their metabolism. Whilst there is little to no information about pres-

862 sure or brine salinity thresholds, neutral pH (pH = 6 – 7) conditions generally corre-
863 spond to the greatest abundance and diversity of microbial life. However, microbial life
864 may exist within the pH range 0 – 11 (Dopffel et al., 2021).

865 In terms of migration, literature on the impact of microbial reactions on hydrogen
866 is scant, with the overwhelming majority of recent and legacy research focused on as-
867 sessing microbial hydrogen generation, consumption and associated environmental risk
868 (e.g. H₂S generation). As generative and destructive processes alter the amount of hy-
869 drogen within a subsurface system, it is conceptually reasonable to consider their role
870 in migration as a moderator of hydrogen flow, whereby the rate of hydrogen transport
871 through a medium influenced by microbes will depend on the kinetics and rates of microbial-
872 hydrogen reactions. Thus, microbial reactions represent an important sink in the migra-
873 tion pathway of hydrogen from depth to the surface. Harris et al. (2007) present one of
874 the few experimental assessments of microbial community metabolism directly within
875 a groundwater environment, and estimate hydrogen consumption rates in-situ injection/withdrawal
876 tests conducted in two geochemically varying, contaminated aquifers. The results of Harris
877 et al. (2007) show that first-order hydrogen consumption rates varied from 0.002 nM h⁻¹
878 for an uncontaminated, aerobic site to 2.5 nM h⁻¹ for a contaminated site where sul-
879 phate reduction was a predominant process. Notably, the hydrogen consumption rate
880 reduced to zero within a denitrifying zone and in the presence of air or an antibiotic mix-
881 ture, thus highlighting potential sensitivity to environmental perturbations on field mi-
882 crobial activities on the timescale of several hours (Harris et al., 2007). These results may
883 be interpreted as meaning the degree to which subsurface microbial activity moderates
884 hydrogen flow may vary on timescales relevant to groundwater flow through the host rock
885 or sediment, e.g. the acidity and salinity of pore fluids in top soils may vary on timescales
886 of hours - days, whereas deeper rocks and aquifers may attenuate environmental signals
887 over thousands of years or longer. Interestingly, Templeton et al. (2024) demonstrate that
888 the alteration of the chemical composition of fluids introduced into geological formations
889 during stimulated hydrogen generation is pivotal for the optimal generation of Fe(III)-
890 enriched secondary mineral phases. Templeton et al. (2024) argue that modifications in
891 fluid chemistry should be strategically engineered to concurrently diminish the micro-
892 bial uptake of H₂ within the stimulated region, whilst maintaining elevated capacities
893 for biogenic hydrogen assimilation in the shallow groundwater systems. The assimi-
894 lation of biogenic hydrogen into shallow groundwater is essential as this will be saturated
895 with oxidising agents such as nitrate, sulfate, and dissolved inorganic carbon. The rec-
896 ommendations of Templeton et al. (2024) serves to mitigate the risk of unintentional hy-
897 drogen emissions into the atmosphere, where it contributes as an indirect greenhouse gas

898 The ability of host rocks to sustain microbial activity on geological timescales may
899 also be dependent on whether the rocks contain sufficient reduced iron and other depen-
900 dent nutrients (Gregory et al., 2019). The compilation of experimental results by Roden
901 and Jin (2011) show that the relationship between microbial yield and the free energy
902 of aerobic and anaerobic metabolism of hydrogen in soils and sediments follow the same
903 linear trend as other compounds, such as glucose, ethanol, formate, acetate, lactate, pro-
904 pionate, butyrate. Roden and Jin (2011)'s results indicate that it is possible to estimate
905 microbial yield values within a factor of 2 (i.e. error = ±100%) using a simple linear re-
906 lationship, although it should be noted that errors are greatest for hydrogen metabolism.
907 The results of Harris et al. (2007) and Roden and Jin (2011) indicate that it may be pos-
908 sible to quantify the role played by subsurface microbial activity as a moderator of hy-
909 drogen transport, however further research is required in this area to determine the re-
910 lationship between subsurface environmental change and the timescale of hydrogen mi-
911 gration.

Microbial hydrogen generation

Process	Reaction	ΔG° kj mol ⁻¹ H ₂	Reference
Fermentation	Multiple pathways that breakdown large organics into smaller organics, e.g., mixed acid fermentation	-54.0 – 24.2	(Thauer et al., 1977; Conrad, 1999) (Schink et al., 2002; Gregory et al., 2019)
Nitrogen fixation (nitrogenase activity)	e.g., C ₆ H ₁₂ O ₆ + 4H ₂ O → 2CH ₃ COO ⁻ + 2HCO ₃ ⁻ + 4H ⁺ + 4H ₂	-18.1	(Thauer et al., 1977; Conrad, 1999)
Anaerobic carbon monoxide oxidation	N ₂ + 8H ⁺ + 8e ⁻ (Fd _{red}) → 2NH ₃ + H ₂ (+Fd _{ox})	-19.9	(Thauer et al., 1977; Conrad, 1999)
Phosphite oxidation	CO + H ₂ O → CO ₂ + H ₂	-46.3	(Thauer et al., 1977; Conrad, 1999)
Acetate oxidation	H ₃ PO ₃ + H ₂ O → H ₃ PO ₄ + H ₂	23.7	(Thauer et al., 1977; Conrad, 1999) (Schink et al., 2002; Gregory et al., 2019)
	$\frac{1}{4}$ CH ₃ COO ⁻ + 14 H ⁺ + $\frac{1}{2}$ H ₂ O → H ₂ + $\frac{1}{2}$ CO ₂		

Microbial hydrogen consumption

Hydrogenotrophic methanogenesis	HCO ₃ ⁻ + H ₂ + $\frac{1}{4}$ H ⁺ → $\frac{1}{4}$ CH ₄ + $\frac{3}{4}$ H ₂ O	-33.9	(Schink et al., 2002; Greening et al., 2016) (Gregory et al., 2019; Dopffel et al., 2021)
Acetogenesis	$\frac{1}{2}$ HCO ₃ ⁻ + H ₂ + $\frac{1}{4}$ H ⁺ → $\frac{1}{4}$ CH ₃ COO ⁻ + 2H ₂ O	-26.1	(Schink et al., 2002; Greening et al., 2016) (Gregory et al., 2019; Dopffel et al., 2021)
Sulphate reduction	$\frac{1}{4}$ SO ₄ ²⁻ + H ₂ + $\frac{1}{4}$ H ⁺ → $\frac{1}{4}$ HS ⁻ + H ₂ O	-38.0	(Schink et al., 2002; Greening et al., 2016) (Gregory et al., 2019; Dopffel et al., 2021)
Sulphur reduction	H ₂ + S → H ₂ S	-33.1	(Schink et al., 2002; Greening et al., 2016) (Gregory et al., 2019; Dopffel et al., 2021)
Iron(III) reduction	2FeOOH + H ₂ + 4H ⁺ → 2Fe ²⁺ + 4H ₂ O	-228.3	(Schink et al., 2002; Greening et al., 2016) (Gregory et al., 2019; Dopffel et al., 2021)
Aerobic hydrogen oxidation	H ₂ + $\frac{1}{2}$ O ₂ → H ₂ O	-237	(Schink et al., 2002; Greening et al., 2016) (Gregory et al., 2019; Dopffel et al., 2021)
Dehalorespiration	Halogenated compounds + H ₂ → dehalogenated compounds + 2HCl	-230 to -187	(Schink et al., 2002; Greening et al., 2016) (Gregory et al., 2019; Dopffel et al., 2021)
Fumarate respiration	H ₂ + fumarate → succinate	-86.2	(Schink et al., 2002; Greening et al., 2016) (Gregory et al., 2019; Dopffel et al., 2021)
Denitrification	$\frac{2}{5}$ NO ₃ ⁻¹ + H ₂ + $\frac{2}{5}$ H ⁺ → $\frac{1}{5}$ N ₂ + $\frac{6}{5}$ H ₂ O	-240.1	(Schink et al., 2002; Greening et al., 2016) (Gregory et al., 2019; Dopffel et al., 2021)

Table 5. Examples of microbial hydrogen generating and consuming reactions. Compiled from (Schink et al., 2002; Greening et al., 2016; Gregory et al., 2019; Dopffel et al., 2021).

Diffusion versus advection

A property that distinguishes hydrogen from other fluids within geological basins is its ability to migrate through rocks occurs via diffusion or advective processes from human to geological timescales. In reality, it is reasonable to assume that hydrogen flow-paths will be a function of both diffusive and advective processes and overall fluid chemistry. However, the ability to predict the behaviour of hydrogen in the subsurface similar to other fluids, such as hydrocarbons and groundwater, remains largely unresolved. The results of Mathiesen et al. (2023); Hutchinson et al. (2024) indicate that pore throat diameter, and therefore capillary entry pressure, exert a primary control on the mode of hydrogen migration, with increasing advective dominance at larger pore throat sizes (i.e. sandstones) and increasing diffusive dominance at smaller pore throat sizes (i.e. shales, evaporites). Lodhia and Clark (2022) approximate hydrogen mobility and buoyancy by solving the Darcy flow equation using a series of steps and use lithological parameters representative of general rock types. Their method may be applied to estimate the basin-scale maximum vertical velocity, v_{max} , of pure advective H₂ gas-flow as the product of mobility and buoyancy, as it accounts for upscaling (due to macro-scale features such as faults and fractures), geological regime (e.g., normal, overpressured or hydrostatic) and geothermal gradient (Lodhia, 2023). However, there is no clear relationship between v_{max} , permeability and porosity (Lodhia & Peeters, 2024). The transition between diffusive and advective flow for pure and multiphase H₂, known as the trans-slip flow boundary, may be calculated using a characteristic Knudsen number value of 0.1 (Hutchinson et al., 2024; Sakhaee-Pour & Alessa, 2022; Roy et al., 2003). We apply data from Strauch et al. (2023) and Fick’s first law to calculate diffusion velocities, v_{diff} , for dry and wetted sandstone, evaporites and clay. Due to a lack of data in the literature, v_{diff} is not calculated for hydrogen migration in carbonates. Calculated basin-scale v_{max} and v_{diff} values are shown on Figure 6A–B and indicate diffusive velocities are several orders of magnitude smaller than advective velocities and that v_{max} decreases exponentially with increasing clay content across all rock types. Advective flow of H₂ becomes less effective at shallow depths (< 400 m) due to the rapid increase in mean free paths. Under multiphase subsurface conditions, advective flow will be impaired due to water occupying and restricting pore space, causing the diffusion-advection boundary to be displaced to larger pore throat sizes (Hutchinson et al., 2024). It is also reasonable to assume that diffusion velocities for hydrogen in carbonates will follow a similar trend to other rock types and be several orders of magnitude smaller than v_{max} values. Hence, calculations of v_{max} , v_{diff} and the position of the diffusion-advection boundary provide an estimate for the timescale and mode of hydrogen migration at different depths in shallow sedimentary basins for a range of rock types. We hypothesise that hydrogen migration is dominated by diffusion at shallow depths and operates on a timescale of < 0.5 cm year⁻¹ for clastic rocks, shale, evaporites and probably carbonates, which decrease by an order of magnitude for water-saturated rocks or sediments. At intermediate depths, the boundary between diffusive and advective flow marks a peak in migration velocity on the timescale of > 0.1 and < 10 m year⁻¹ for most clastic and carbonate rocks, with the exception of dolomites which have advective velocities from ~ 100–1000 m year⁻¹. The boundary between diffusive and advective hydrogen flow is not uniform across different rock types, such that multiphase conditions cause displacement towards more coarsely grained rocks and an increased depth envelope for diffusive migration. Advective velocities decrease with depth due to the reduction in pore throat sizes and corresponding increase in capillary entry pressures required for hydrogen flow. Furthermore, whilst increased clay content will affect the timescale of advective flow, the effect on diffusion is minimal.

Future experimental research should focus on improving understanding of porosity and water saturation relationships relevant for hydrogen, as due to a lack of data in the literature, Lodhia and Clark (2022) apply estimates of oil-water and gas-water systems. Future experimental studies may also focus on testing both the robustness of Lodhia and Clark (2022)’s approximations and our hypotheses.

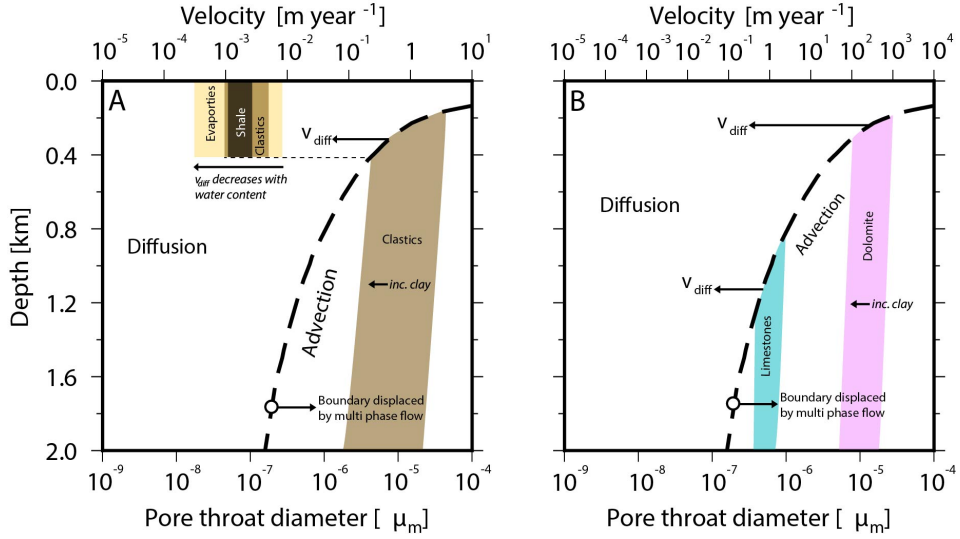


Figure 6. Maximum vertical velocity (v_{max}) and diffusion velocity (v_{diff}) calculated for various rock types using the method of Lodhia and Clark (2022) and data from Hantschel and Kauerauf (2009) and Strauch et al. (2023), respectively. A = velocity v_{max} and v_{diff} for clastic rocks. Dashed horizontal line indicates the maximum depth of transition between advective and diffusive migration for pure H₂. v_{diff} decreases with increasing water content due to a rapid increase in mean free paths (i.e., increased collisions between H₂ and water molecules) whilst v_{max} decreases with increasing clay content due to increased capillary entry pressure associated with decreasing pore throat diameter (e.g. Hutchinson et al. (2024)). B = v_{max} for carbonate rocks. We do not calculate v_{diff} values for carbonates due to a lack of data within the literature, however assume these to follow a similar trend to clastic rocks and be several orders of magnitude smaller than corresponding v_{max} values (see labelled arrows). Curved dashed line = diffusion-advection boundary for pure H₂ calculated using a Knudsen number of 0.1 (Hutchinson et al., 2024). This boundary is displaced to larger pore throat sizes for multiphase subsurface flow as indicated by circled arrows.

Discussion

The migration of hydrogen through the subsurface is a topic seldom addressed directly, yet is critical for exploration and geological storage investigations. To understand the dynamics of the subsurface hydrogen cycle within sedimentary basins and Earth's surface, we must take a holistic view of its supply, emission and intermediate processes.

Within geological basins, long-term hydrogen supply from the radiolysis of water within crystalline basement, Archean - Proterozoic cratonic rocks and other hydrogen abundant mafic igneous rocks will remain steady over geological timescales. However, hydrogen migration pathways will be disproportionately affected by specific processes operating within small regions within sedimentary basins and Earth's crust, such as microbial reactions in soil or regolith, advection of fluids along faults and 'trapping' on timescales relative to humans by wet or evaporitic sediments. Environmental factors, such as salinity and temperature may change the dynamics of subsurface hydrogen systems rapidly, for example a saline aquifer changing from a barrier to a carrier due to an influx of fresh meteoric water following heavy rainfall. Hydrogen supply rates within generative systems will be primarily controlled by the availability of fresh water, such as rainfall on ophiolitic systems or groundwater contact with buried igneous rocks.

The rate of diffusive migration of hydrogen from crystalline rocks into surrounding sediments will operate on timescales of 1–1000 years (Figure 2), and be controlled primarily by grain size and temperature. Experimental results from the literature indicate that native hydrogen entrained within the mineral structure of crystalline rocks within the shallow Earth may diffuse on geological timescales from the most common rock forming minerals. Geochemical data obtained by Parnell and Blamey (2017) indicate that common felsic lithologies, such as granites, gneiss and conglomerates of Archean - Proterozoic (> 1600 Ma) age consistently contain an order of magnitude greater hydrogen in their entrained fluid than very young (< 200 Ma) granites. Parnell and Blamey (2017) found that sedimentary rocks containing clasts of old basement also included a greater proportion of hydrogen than young granites and hypothesise that a signature of hydrogen in the basement could be conferred to the sediment and that modern sediment derived from old and young basement retains the signature of more or less hydrogen, respectively (Figure 7). It should be noted however that the experimental results summarised by Parnell and Blamey (2017) refer to bulk lithologies whereas those of Farver (2010) refer to individual minerals (e.g. olivine and quartz). Furthermore, the preservation of high hydrogen abundances within fluid inclusions and mineralised veins in ancient granites has been observed (Bourdet et al., 2023). Hence, diffusion from enriched Archean - Proterozoic crystalline basement and their derived sedimentary products, e.g., conglomerates, may supply a 'background' hydrogen flux to overlying sedimentary basin rocks on geological timescales. This is consistent with the widely documented observation of higher hydrogen fluxes in sedimentary basins in continental cratonic regions underlain by Archean - Proterozoic basement (e.g. Zgonnik (2020); Moretti, Brouilly, et al. (2021)). In the case of rapidly cooled upper mantle rocks, e.g. MORBs, volcanic glasses, pillow lavas, however, grain sizes may be many orders of magnitude smaller than their continental counterparts and within the nanometre scale (e.g., Schlinger et al. (1988)). Hence, hydrogen diffusivity in rapidly cooled crystalline rocks and at MOR settings will be significantly faster than in continental settings and potentially only a few orders of magnitude slower than the lower temperature ranges of diffusivity experiments, i.e. 100 Ka - Ma or faster. This is significant, since the age of most oceanic crustal rocks is < 60 Ma (Seton et al., 2020), hydrogen diffusion within oceanic crustal rocks will operate on the same timescale as the age of rocks themselves and provide a mechanism for the degassing of mantle hydrogen to the surface and oceans. Figure 7 summarises the characteristic migration timescales for hydrogen transport through different parts of a sedimentary basin as described in this article.

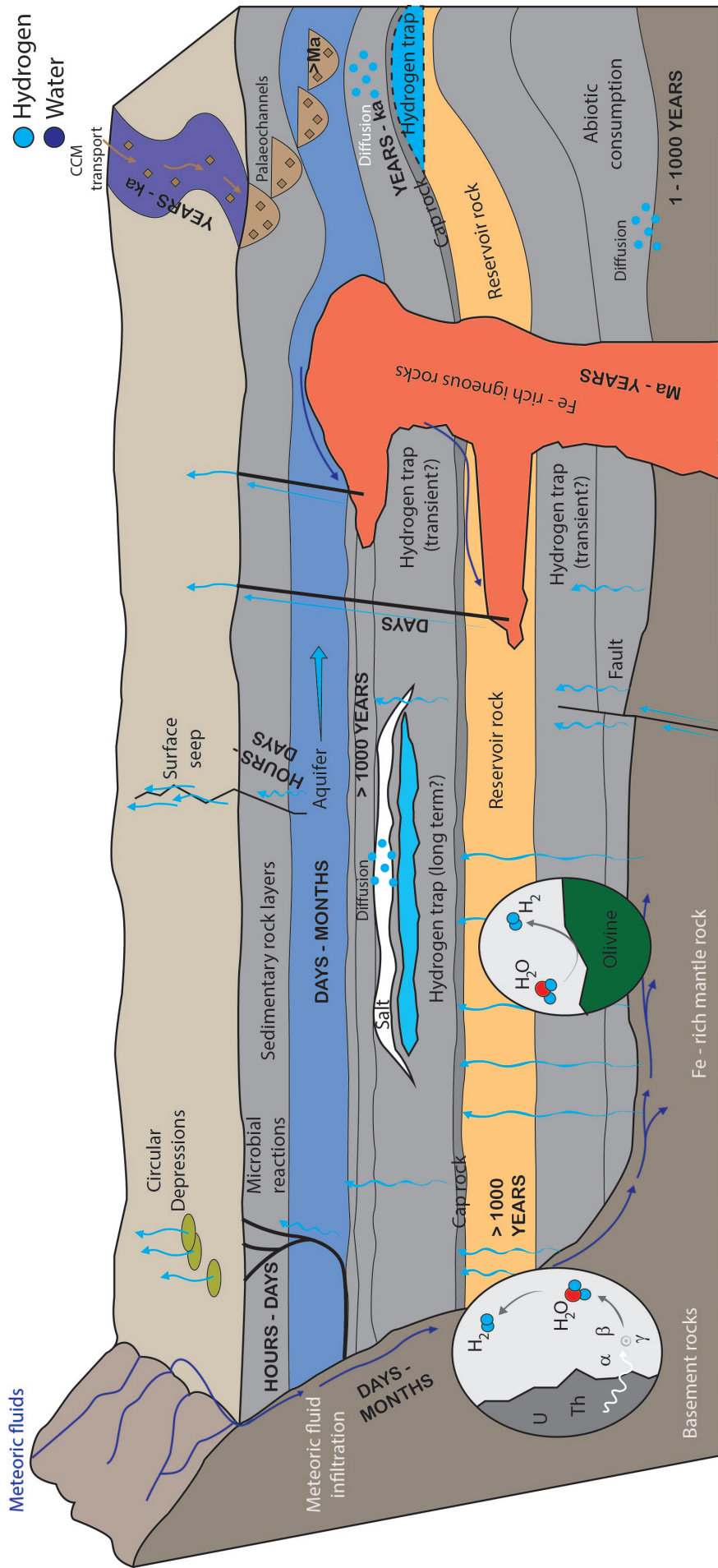


Figure 7. Conceptual method for modelling workflow, migration and indicative timescales through sedimentary basins. Blue arrows indicate advective transport of hydrogen. Fe-rich lithologies (e.g. granites) characterise Archean - Proterozoic continental crystalline basement within cratonic regions and igneous intrusive rocks. Diffusion through geological barriers to hydrogen migration, e.g. salt and igneous intrusions may limit hydrogen migration by thousands to millions of years, depending on mineralogy and lithology (Farver, 2010; Parnell & Blamey, 2017). Continental clastic material (CCM) derived from terrains enriched in hydrogen (e.g. Archean - Proterozoic basement) is believed to be responsible for the provenance of high hydrogen concentrations in some sedimentary basin rocks (Parnell & Blamey, 2017). The transport of CCM (brown diamonds and arrows) by fluvial systems and accumulation in palaeochannel deposits is shown for conceptual purposes. Modified from Hand (2023)

1018 Whilst faulting and fluid flow have been extensively reviewed in the literature, their
 1019 impact on hydrogen migration have only recently gained significant attention. Obser-
 1020 vations of hydrogen pulses prior to seismic activity are not well documented, but can be
 1021 analogous to increased CO₂ emissions possibly due to enhanced porosity of the soil due
 1022 to faulting, and accelerated water rock interactions and soil gas emission within the fault
 1023 zone (e.g., Z. Liu et al. (2023)). Early work by by Wakita et al. (1980) hypothesised the
 1024 production of hydrogen by fault movement, based on measurements of elevated hydro-
 1025 gen concentrations (> 3% by volume) around active fault zones in southwestern Japan
 1026 compared to background measurements of ~ 0.5 ppm. Su et al. (1992) identified the po-
 1027 tential reduction in strength of crystalline minerals (e.g., calcite, dolomite, antigorite)
 1028 due to hydrogen infiltration at low pressures, leading to the weakening of rocks and ini-
 1029 tiation of faulting. Hydrogen gas measurements and particle size distribution analyses
 1030 by Niwa et al. (2011) within an active fault zone indicate that hydrogen gas mostly mi-
 1031 grated in permeable fracture zones by advection with groundwater. Firstov and Shirokov
 1032 (2005) measured seven pulses of hydrogen discharge against background levels in a fault
 1033 zone trending parallel the Kuril - Kamchatka geostructural zone, Russia, from 1999–
 1034 2003. Hydrogen pulses preceding seismic events lasted from 1.5–6 hours and were 2–
 1035 14 times higher than measured background levels. Firstov and Shirokov (2005) found
 1036 that < 80% earthquakes with $M_W \geq 5.6$ in the southern Kamchatka region occurred
 1037 within one month of measured hydrogen pulses and considered such events as short-term
 1038 earthquake precursors. In recent years, the migration of natural hydrogen from deep crustal
 1039 sources along kilometre-scale faults which penetrate crystalline basement have been recorded
 1040 in several locations across the world (e.g., Brazil, France, Mali) (Prinzhofer et al., 2018;
 1041 Deronzier & Giouse, 2020; Donzé et al., 2020; Rezaee, 2021; Frery, Langhi, et al., 2021;
 1042 Lefevre et al., 2021, 2022).

1043 **Recent hydrogen discoveries and possible importance to migration path-** 1044 **ways**

1045 Following the landmark discovery of natural hydrogen at Bourakebougou in Mali
 1046 by Prinzhofer et al. (2018), subsequent research has uncovered numerous hydrogen de-
 1047 posits worldwide. In this section, we review several recent discoveries and examine po-
 1048 tential relationships between gas composition and fluid migration pathways.

1049 A regional geochemistry study by Lévy, Boka-Mene, et al. (2023) in Albania and
 1050 Kosovo focused on natural springs, revealing a site in northern Kosovo with a hydrogen
 1051 concentration of 16%, pointing to serpentinisation of peridotites as a hydrogen source.
 1052 Notably, this study found no correlation between hydrogen and helium concentrations
 1053 but did observe substantial organic and crustal contributions (CH₄ and N₂). Contrast-
 1054 ingly, recent data from South Australia and direct measurements from the Bulqizë chromite
 1055 mine in Albania report significant hydrogen outgassing, with H₂ concentrations > 80%
 1056 and varying but minor N₂, CO₂ and CH₄ components (Goh, 2023; Hydrogen, 2023; Truche
 1057 et al., 2024; Yeo, 2023). Interestingly, whilst the results of Lévy, Boka-Mene, et al. (2023)
 1058 indicated no a clear connection between hydrogen and helium in the context of serpen-
 1059 tinisation, Karolyté et al. (2022) documented He-rich hydrocarbon gases in South Africa’s
 1060 Witwatersrand Basin, where the scarcity of mafic and ultramafic minerals capable of ser-
 1061 pentinisation suggests radiolytic hydrogen production as the predominant mechanism.
 1062 Despite the detection of hydrogen alongside CH₄ and N₂ in both scenarios, the system
 1063 described by Karolyté et al. (2022) is not associated with hydrocarbon source rocks. Trans-
 1064 portation over vast distances and a significant degree of interaction with groundwater
 1065 dilute He and lower H/He ratios (Ballentine & Lollar, 2002; Gilfillan et al., 2008). Hence,
 1066 observed He concentrations in the Witwatersand Basin by Karolyté et al. (2022) may
 1067 be explained by long periods of quiescence for He accumulation within a closed system,
 1068 characterised by its hydrogeological systems being isolated and He preservation.

1069 These examples highlight the rapid conversion of hydrogen to methane in surface
 1070 environments and the influence of gas composition on migration pathways, particularly
 1071 the impact of helium content on gas mixture compositions over geological timeframes.
 1072 Prinzhofer and Cacas-Stentz (2023) present theoretical analyses suggesting that advective
 1073 leakage of hydrogen-bearing gases out of subsurface reservoirs affects their overall
 1074 composition, leading to an increase in nitrogen and methane content at the expense of
 1075 hydrogen. Their findings suggest a dichotomy where hydrogen, though renewable on human
 1076 scales, is diluted on geological timescales, while helium, due to its inert nature, accumulates
 1077 over similar periods. Their models demonstrate the rapid formation of natural hydrogen
 1078 deposits, with instances of H₂-dominant gas accumulations \sim 500 years
 1079 old in Mali, evolving to CH₄-dominant mixtures \sim 40 ka old in Turkey, and N₂-rich variants
 1080 within timescales of millions of years, exemplified by the Amadeus Basin in Australia
 1081 (Boreham et al., 2021).

1082 These analyses indicate that H₂-rich gas subsurface accumulations are dependent
 1083 on recent or ongoing hydrogen generation, whilst fossil accumulations are characterised
 1084 by lower H₂ abundances and greater organic and crustal component abundancies. The
 1085 relationship between fluid migration and helium is paradoxical, given that for high He
 1086 concentrations to be preserved alongside high H₂ concentrations (e.g. Hydrogen (2023)),
 1087 migration must be rapid enough to prevent dilution whilst the isolation of fluids over billions
 1088 of years could allow He to accumulate whilst H₂ is lost (e.g. Karolyt  et al. (2022)).
 1089 The relationship between surface gas seep compositions and migration pathways is more
 1090 nuanced, given that microbial methanogenesis (Table 5) is depth-dependent (e.g., Truche
 1091 et al. (2024)). Hydrogen consumption within the shallowest levels of the subsurface (<
 1092 1 m) may imprint a diurnal variation onto otherwise long-lived high-concentration (>
 1093 50%) H₂ signals (e.g. Myagkiy, Moretti, and Brunet (2020)). For high H₂ concentrations
 1094 to be preserved to the surface, we hypothesise that fluid migration pathways operate on
 1095 both short timescales and lengthscales such that the opportunity for environmental hydrogen
 1096 uptake is severely limited. However, we propose that seeps characterised by low
 1097 hydrogen concentrations (< 20%, e.g. L vy, Boka-Mene, et al. (2023)) typify migration
 1098 pathways over greater distances and timescales, such as basin-scale transport along faults
 1099 and fractures, whereby substantial amounts of hydrogen are lost due to microbial consumption
 1100 and other processes.

1101 Lefevre et al. (2024) investigates natural hydrogen occurrences in the Paris Basin
 1102 using Optical Character Recognition (OCR) technology to analyse historical drilling records
 1103 by leveraging the CVAGeoDB database, which includes well logs, mudlogs, and End Drilling
 1104 Reports (EDRs). Their analysis revealed several hydrogen-bearing wells, with the highest
 1105 concentration (52 vol%) found in the Dogger aquifer. The wells are primarily located
 1106 along the Bray Fault, indicating structural influences on hydrogen distribution. Lefevre
 1107 et al. (2024) demonstrates OCR’s effectiveness in reassessing historical data for hydrogen
 1108 exploration and highlights the Paris Basin’s potential as a hydrogen-rich geological
 1109 province.

1110 Conclusion

1111 Hydrogen within the subsurface remains elusive. While entrenched into Earth during
 1112 planetary formation, the exchange of hydrogen between materials is prevalent during
 1113 subsurface processes at all depths. Significant advances in understanding the distribution
 1114 and generation of natural hydrogen have been made in recent literature, however large
 1115 gaps remain in our understanding of large-scale hydrogen migration. The timescale of
 1116 hydrogen migration throughout Earth varies from billions of years to days, and is dependent
 1117 on a wide range of lithological and environmental factors. Grain size, temperature and
 1118 fluid salinity exert important controls on hydrogen diffusivity in crystalline and
 1119 sedimentary rocks. Diffusive and advective migration of hydrogen vary by several
 1120 orders of magnitude, however operate on timescales of < 0.5 cm to m per > 1000 m

per year, respectively. Fluid migration along faults and fractures is controlled by rock properties, subsurface stress regimes and groundwater properties. The phenomena of gas-induced fault opening and hydrogen pulses associated with seismic activity require further research. Microbial reactions moderate subsurface hydrogen flow by altering mass balance on differing timescales related to depth and environmental factors. Understanding the transition between diffusive and advective flow of hydrogen and multiphase fluids within different rock types in the subsurface remains a key challenge.

Acknowledgments

This work was supported by the Impossible Without You program, Hydrogen Energy Systems Future Science Platform and Hydrogen Industry Mission, CSIRO. The authors would like to thank Trevor Rapson for his initial suggestion to write this review. We thank Axel Suckow and Joel Sarout for reviewing this manuscript. Thanks are also given to Kate Holland for her support of this project and to our colleagues and associates for their discussions.

Open Research

The data files used in this paper are available at Lodhia (2023) and Lodhia and Clark (2022).

Declarations

The authors declare no conflicts of interest.

References

- Abrajano, T. A., Sturchio, N. C., Bohlke, J. K., Lyon, G. L., Poreda, R. J., & Stevens, C. M. (1988). Methane-hydrogen gas seeps, zambales ophiolite, philippines: Deep or shallow origin? *Chemical Geology*, *71*, 211-222.
- Abrajano, T. A., Sturchio, N. C., Kennedy, B. M., Lyon, G. L., Muehlenbachs, K., & Bohlke, J. K. (1990). *Geochemistry of reduced gas related to serpentinization of the zambales ophiolite, philippines* (Vol. 5).
- Allègre, C., Staudacher, T., & P., M. S., Kurz, (1983). Constraints on evolution of earth's mantle from rare gas systematics. *Nature*, *303*, 762-766. doi: <https://doi.org/10.1038/303762a0>
- Allègre, C. J., Moreira, M., & Staudacher, T. (1995). 4He/³He dispersion and mantle convection. *Geophysical Research Letters*, *22*, 2325-2328. doi: 10.1029/95GL02307
- Al-Yaseri, A., Yekeen, N., Mahmoud, M., Kakati, A., Xie, Q., & Giwelli, A. (2022). Thermodynamic characterization of h₂-brine-shale wettability: Implications for hydrogen storage at subsurface. *International Journal of Hydrogen Energy*, *47*, 22510-22521. doi: 10.1016/j.ijhydene.2022.05.086
- Anderson, R. T., Chapelle, F. H., & Lovley, D. R. (1998). Evidence against hydrogen-based microbial ecosystems in basalt aquifers. *Science*, *281*, 976-977. doi: 10.1126/science.281.5379.976
- Andresen, K. J., & Huuse, M. (2011). 'bull's-eye' pockmarks and polygonal faulting in the lower congo basin: Relative timing and implications for fluid expulsion during shallow burial. *Marine Geology*, *279*, 111-127. doi: 10.1016/j.margeo.2010.10.016
- Bagreev, A., Menendez, J. A., Dukhno, I., Tarasenko, Y., & Bandosz, T. J. (2004). Bituminous coal-based activated carbons modified with nitrogen as adsorbents of hydrogen sulfide. *Carbon*, *42*, 469-476. doi: 10.1016/j.carbon.2003.10.042

- 1167 Ballentine, C. J., & Lollar, B. S. (2002). *Regional groundwater focusing of nitrogen*
 1168 *and noble gases into the hugoton-panhandle giant gas field, usa.*
- 1169 Bania, T. M., Rood, R. T., & Balsler, D. S. (2002). The cosmological density of
 1170 baryons from observations of 3 he + in the milky way. *Nature*, *415*, 54-57. doi:
 1171 <https://doi.org/10.1038/415054a>
- 1172 Berta, M., Dethlefsen, F., Ebert, M., Schäfer, D., & Dahmke, A. (2018). Geochem-
 1173 ical effects of millimolar hydrogen concentrations in groundwater: An exper-
 1174 imental study in the context of subsurface hydrogen storage. *Environmental*
 1175 *Science and Technology*, *52*, 4937-4949. doi: 10.1021/acs.est.7b05467
- 1176 Bodnar, R. J., Azbej, T., Becker, S. P., Cannatelli, C., Fall, A., & Severs, M. J.
 1177 (2013). Whole earth geohydrologic cycle, from the clouds to the core: The dis-
 1178 tribution of water in the dynamic earth system. *Special Paper of the Geological*
 1179 *Society of America*, *500*, 431-461. doi: 10.1130/2013.2500(13)
- 1180 Boreham, C. J., Edwards, D. S., Czado, K., Rollet, N., Wang, L., van der Wielen, S.,
 1181 ... Henson, P. A. (2021). Hydrogen in australian natural gas: occurrences,
 1182 sources and resources. *The APPEA Journal*, *61*, 163. doi: 10.1071/aj20044
- 1183 Boreham, C. J., Edwards, D. S., Feitz, A. J., Murray, A. P., Mahlstedt, N., & Hors-
 1184 field, B. (2023). Modelling of hydrogen gas generation from overmature organic
 1185 matter in the cooper basin, australia. *The APPEA Journal*, *63*, S351-S356.
 1186 doi: 10.1071/aj22084
- 1187 Boschi, L., Becker, T. W., & Steinberger, B. (2007). Mantle plumes: Dynamic mod-
 1188 els and seismic images. *Geochemistry, Geophysics, Geosystems*, *8*. doi: 10
 1189 .1029/2007GC001733
- 1190 Bouhifd, M. A., Jephcoat, A. P., Heber, V. S., & Kelley, S. P. (2013). Helium in
 1191 earth's early core. *Nature Geoscience*, *6*, 982-986. doi: 10.1038/ngeo1959
- 1192 Bourdet, J., Piane, C. D., Wilske, C., Mallants, D., Suckow, A., Questiaux, D.,
 1193 ... Aleshin, M. (2023). Natural hydrogen in low temperature geofluids in
 1194 a precambrian granite, south australia. implications for hydrogen genera-
 1195 tion and movement in the upper crust. *Chemical Geology*, *638*, 1-18. doi:
 1196 <https://doi.org/10.1016/j.chemgeo.2023.121698>
- 1197 Burnside, N. M., Shipton, Z. K., Dockrill, B., & Ellam, R. M. (2013). Man-made
 1198 versus natural co2 leakage: A 400 k.y. history of an analogue for engineered
 1199 geological storage of co2. *Geology*, *41*, 471-474. doi: 10.1130/G33738.1
- 1200 Capitano, F. A., Nebel, O., Cawood, P. A., Weinberg, R. F., & Chowdhury, P.
 1201 (2019). Reconciling thermal regimes and tectonics of the early earth. *Geology*,
 1202 *47*, 923-927. doi: 10.1130/G46239.1
- 1203 Capitano, F. A., Nebel, O., Moyen, J. F., & Cawood, P. A. (2022). Craton for-
 1204 mation in early earth mantle convection regimes. *Journal of Geophysical Re-*
 1205 *search: Solid Earth*, *127*. doi: 10.1029/2021JB023911
- 1206 Cartwright, J. (2011). *Diagenetically induced shear failure of fine-grained sedi-*
 1207 *ments and the development of polygonal fault systems* (Vol. 28). doi: 10.1016/j
 1208 .marpetgeo.2011.06.004
- 1209 Cartwright, J., James, D., & Bolton, A. (2003). The genesis of polygonal fault sys-
 1210 tems: A review. *Geological Society Special Publication*, *216*, 223-234. doi: 10
 1211 .1144/GSL.SP.2003.216.01.15
- 1212 Chabab, S., Kerkache, H., Bouchkira, I., Poulain, M., Baudouin, O., Édouard Moine,
 1213 ... Cézac, P. (2024). Solubility of h2 in water and nacl brine under subsurface
 1214 storage conditions: Measurements and thermodynamic modeling. *International*
 1215 *Journal of Hydrogen Energy*, *50*, 648-658. doi: 10.1016/j.ijhydene.2023.10.290
- 1216 Chabab, S., Théveneau, P., Coquelet, C., Corvisier, J., & Paricaud, P. (2020).
 1217 Measurements and predictive models of high-pressure h2 solubility in brine
 1218 (h2o+nacl) for underground hydrogen storage application. *International Jour-*
 1219 *nal of Hydrogen Energy*, *45*, 32206-32220. doi: 10.1016/j.ijhydene.2020.08.192
- 1220 Conrad, R. (1999). Contribution of hydrogen to methane production and control of
 1221 hydrogen concentrations in methanogenic soils and sediments. *FEMS Microbi-*

- 1222 *ology Ecology*, 28, 193-202. doi: 10.1111/j.1574-6941.1999.tb00575.x
- 1223 Cooke, R. J., Pettini, M., Jorgenson, R. A., Murphy, M. T., & Steidel, C. C. (2014).
 1224 Precision measures of the primordial abundance of deuterium. *Astrophysical*
 1225 *Journal*, 781. doi: 10.1088/0004-637X/781/1/31
- 1226 Cox, S. F., & Etheridge, M. A. (1989). Coupled grain-scale dilatancy and mass
 1227 transfer during deformation at high fluid pressures: examples from mount lyell,
 1228 tasmania. *Journal of Structural Geology*, 11, 147-162.
- 1229 Craig, H., & Lupton, J. (1976). Primordial neon, helium, and hydrogen in oceanic
 1230 basalts. *Earth and Planetary Science Letters*, 31, 369-385. doi: [https://doi](https://doi.org/10.1016/0012-821X(76)90118-7)
 1231 [.org/10.1016/0012-821X\(76\)90118-7](https://doi.org/10.1016/0012-821X(76)90118-7)
- 1232 Debaille, V., O'Neill, C., Brandon, A. D., Haenecour, P., Yin, Q. Z., Mattielli, N., &
 1233 Treiman, A. H. (2013). Stagnant-lid tectonics in early earth revealed by 142nd
 1234 variations in late archean rocks. *Earth and Planetary Science Letters*, 373,
 1235 83-92. doi: 10.1016/j.epsl.2013.04.016
- 1236 de Blok, W. J., Fortuin, J. M. H., & Vermeulen, D. P. (1982). Bestimmung des dif-
 1237 fusionskoeffizienten von wasserstoff in wasser und w isserigen polymerliisungen
 1238 nach der cbs-methode measurement of the diffusion coefficient of hydrogen in
 1239 water ca and aqueous polymer solutions according to the cbs-method. *Wirme*
 1240 *und Stofffibertragung*, 17, 11-16.
- 1241 Demouchy, S. (2010). Diffusion of hydrogen in olivine grain boundaries and im-
 1242 plications for the survival of water-rich zones in the earth's mantle. *Earth and*
 1243 *Planetary Science Letters*, 295, 305-313. doi: 10.1016/j.epsl.2010.04.019
- 1244 Demouchy, S., & Mackwell, S. (2006). Mechanisms of hydrogen incorporation and
 1245 diffusion in iron-bearing olivine. *Physics and Chemistry of Minerals*, 33, 347-
 1246 355. doi: 10.1007/s00269-006-0081-2
- 1247 Deronzier, J. F., & Giouse, H. (2020). Vaux-en-bugey (ain, france): The first
 1248 gas field produced in france, providing learning lessons for natural hy-
 1249 drogen in the sub-surface? *BSGF - Earth Sciences Bulletin*, 191. doi:
 1250 10.1051/bsgf/2020005
- 1251 Deville, E., & Prinzhofer, A. (2016). The origin of n2-h2-ch4-rich natu-
 1252 ral gas seepages in ophiolitic context: A major and noble gases study of
 1253 fluid seepages in new caledonia. *Chemical Geology*, 440, 139-147. doi:
 1254 10.1016/j.chemgeo.2016.06.011
- 1255 Dodd, M. S., Wang, H., Li, C., Towner, M., Thomson, A. R., Slack, J. F., ... Pap-
 1256 ineau, D. (2022). Abiotic anoxic iron oxidation, formation of archean banded
 1257 iron formations, and the oxidation of early earth. *Earth and Planetary Science*
 1258 *Letters*, 584. doi: 10.1016/j.epsl.2022.117469
- 1259 Donzé, F. V., Truche, L., Namin, P. S., Lefeuvre, N., & Bazarkina, E. F. (2020).
 1260 Migration of natural hydrogen from deep-seated sources in the são fran-
 1261 cisco basin, brazil. *Geosciences (Switzerland)*, 10, 1-16. doi: 10.3390/
 1262 geosciences10090346
- 1263 Dopffel, N., Jansen, S., & Gerritse, J. (2021). *Microbial side effects of underground*
 1264 *hydrogen storage – knowledge gaps, risks and opportunities for successful imple-*
 1265 *mentation* (Vol. 46). Elsevier Ltd. doi: 10.1016/j.ijhydene.2020.12.058
- 1266 Dutta, A., Gupta, S. D., Gupta, A., Sarkar, J., Roy, S., Mukherjee, A., & Sar, P.
 1267 (2018). Exploration of deep terrestrial subsurface microbiome in late creta-
 1268 ceous deccan traps and underlying archean basement, india. *Scientific Reports*,
 1269 8. doi: 10.1038/s41598-018-35940-0
- 1270 Eichhubl, P., & Boles, J. R. (2000). Focused fluid flow along faults in the mon-
 1271 terey formation, coastal california. *GSA Bulletin*, 1667-1679. Retrieved from
 1272 [http://pubs.geoscienceworld.org/gsa/gsabulletin/article-pdf/112/](http://pubs.geoscienceworld.org/gsa/gsabulletin/article-pdf/112/11/1667/3383642/i0016-7606-112-11-1667.pdf)
 1273 [11/1667/3383642/i0016-7606-112-11-1667.pdf](http://pubs.geoscienceworld.org/gsa/gsabulletin/article-pdf/112/11/1667/3383642/i0016-7606-112-11-1667.pdf)
- 1274 Escudero, C., Oggerin, M., & Amils, R. (2018). The deep continental subsurface: the
 1275 dark biosphere. *International Microbiology*, 21, 3-14. doi: 10.1007/s10123-018-
 1276 -0009-y

- 1277 Farough, A., Moore, D. E., Lockner, D. A., & Lowell, R. P. (2016). Evolution of
1278 fracture permeability of ultramafic rocks undergoing serpentinization at hy-
1279 drothermal conditions: An experimental study. *Geochemistry, Geophysics,*
1280 *Geosystems, 17*, 44-55. doi: 10.1002/2015GC005973
- 1281 Farquhar, J., Wing, B., McKeegan, K., Harris, J., Cartigny, P., & Thiemens, M.
1282 (2002). Mass-independent sulfur of inclusions in diamond and sulfur recycling
1283 on early earth. *Science, 298*, 2369-2372.
- 1284 Farver, J. R. (2010). Oxygen and hydrogen diffusion in minerals. *Reviews in Miner-*
1285 *alogy and Geochemistry, 72*, 447-507. doi: 10.2138/rmg.2010.72.10
- 1286 Faulkner, D. R., Jackson, C. A., Lunn, R. J., Schlische, R. W., Shipton, Z. K., Wib-
1287 berley, C. A., & Withjack, M. O. (2010). A review of recent developments
1288 concerning the structure, mechanics and fluid flow properties of fault zones.
1289 *Journal of Structural Geology, 32*, 1557-1575. doi: 10.1016/j.jsg.2010.06.009
- 1290 Ferrell, R. T., & Himmelblau, D. M. (1967). Diffusion coefficients of hydrogen and
1291 helium in water. *AIChE Journal, 13*, 702-708. doi: 10.1002/aic.690130421
- 1292 Firstov, P., & Shirokov, V. (2005). Dynamics of molecular hydrogen and its relation
1293 to deformational processes at the petropavlovsk-kamchatskii geodynamic test
1294 site: Evidence from observations in 1999–2003. *Geochemistry International,*
1295 *43*, 1056-1064.
- 1296 French, S. W., & Romanowicz, B. (2015). Broad plumes rooted at the base of the
1297 earth’s mantle beneath major hotspots. *Nature, 525*, 95-99. doi: 10.1038/
1298 nature14876
- 1299 Frery, E., Fryer, P., Kurz, W., Nguyen, A., Sissmann, O., Uysal, T., & Zhao, J.
1300 (2021). Episodicity of structural flow in an active subduction system, new in-
1301 sights from mud volcano’s carbonate veins – scientific ocean drilling expedition
1302 iodp 366. *Marine Geology, 434*. doi: 10.1016/j.margeo.2021.106431
- 1303 Frery, E., Gratier, J. P., Ellouz-Zimmerman, N., Loiselet, C., Braun, J., De-
1304 schamps, P., ... Swennen, R. (2015). Evolution of fault permeability dur-
1305 ing episodic fluid circulation: Evidence for the effects of fluid-rock interac-
1306 tions from travertine studies (utah-usa). *Tectonophysics, 651*, 121-137. doi:
1307 10.1016/j.tecto.2015.03.018
- 1308 Frery, E., Langhi, L., Maison, M., & Moretti, I. (2021). Natural hydrogen seeps
1309 identified in the north perth basin, western australia. *International Journal of*
1310 *Hydrogen Energy, 46*, 31158-31173. doi: 10.1016/j.ijhydene.2021.07.023
- 1311 Frisch, H. L. (1957). The time lag in diffusion. *The Journal of Physical Chemistry,*
1312 *61*, 93-95. Retrieved from <https://pubs.acs.org/sharingguidelines> doi:
1313 10.1021/j150547a018
- 1314 Garnero, E. J., McNamara, A. K., & Shim, S. H. (2016). *Continent-sized anoma-*
1315 *lous zones with low seismic velocity at the base of earth’s mantle* (Vol. 9). Na-
1316 ture Publishing Group. doi: 10.1038/ngeo2733
- 1317 Gautheron, C., & Moreira, M. (2002). Helium signature of the subcontinental litho-
1318 spheric mantle. *Earth and Planetary Science Letters, 199*, 39-47. Retrieved
1319 from www.elsevier.com/locate/epsl
- 1320 Geiss, J., & Gloeckler, G. (1998). Abundances of deuterium and helium-3 in the pro-
1321 tosolar cloud. In N. Prantzos, M. Tosi, & R. V. Steiger (Eds.), (1st ed., Vol. 4,
1322 p. 239-250). Springer.
- 1323 Gerya, T. V., Stern, R. J., Baes, M., Sobolev, S. V., & Whattam, S. A. (2015).
1324 Plate tectonics on the earth triggered by plume-induced subduction initiation.
1325 *Nature, 527*, 221-225. doi: 10.1038/nature15752
- 1326 Geymond, U., Ramanaidou, E., Lévy, D., Ouaya, A., & Moretti, I. (2022).
1327 Can weathering of banded iron formations generate natural hydrogen?
1328 evidence from australia, brazil and south africa. *Minerals, 12*. doi:
1329 10.3390/min12020163
- 1330 Gilfillan, S. M., Ballentine, C. J., Holland, G., Blagburn, D., Lollar, B. S.,
1331 Stevens, S., ... Cassidy, M. (2008). The noble gas geochemistry of nat-

- 1332 ural co₂ gas reservoirs from the colorado plateau and rocky mountain
1333 provinces, usa. *Geochimica et Cosmochimica Acta*, 72, 1174-1198. doi:
1334 10.1016/j.gca.2007.10.009
- 1335 Goh, J. (2023). *Gold hydrogen detects significant concentrations of hydrogen and*
1336 *helium at ramsay 1 well.* Retrieved from [https://www.proactiveinvestors](https://www.proactiveinvestors.com.au/companies/news/1031450/gold-hydrogen-detects-significant-concentrations-of-hydrogen-and-helium-at-ramsay-1-well-1031450.html)
1337 [.com.au/companies/news/1031450/gold-hydrogen-detects-significant](https://www.proactiveinvestors.com.au/companies/news/1031450/gold-hydrogen-detects-significant-concentrations-of-hydrogen-and-helium-at-ramsay-1-well-1031450.html)
1338 [-concentrations-of-hydrogen-and-helium-at-ramsay-1-well-1031450](https://www.proactiveinvestors.com.au/companies/news/1031450/gold-hydrogen-detects-significant-concentrations-of-hydrogen-and-helium-at-ramsay-1-well-1031450.html)
1339 [.html](https://www.proactiveinvestors.com.au/companies/news/1031450/gold-hydrogen-detects-significant-concentrations-of-hydrogen-and-helium-at-ramsay-1-well-1031450.html)
- 1340 Gonnermann, H. M., & Mukhopadhyay, S. (2007). Non-equilibrium degassing and
1341 a primordial source for helium in ocean-island volcanism. *Nature*, 449, 1037-
1342 1040. doi: 10.1038/nature06240
- 1343 Graham, D. W. (2002). Noble gas isotope geochemistry of mid-ocean ridge and
1344 ocean island basalts: Characterization of mantle source reservoirs. *Reviews in*
1345 *Mineralogy and Geochemistry*, 47. doi: 10.2138/rmg.2002.47.8
- 1346 Gratier, J.-P., & Gueydan, F. (2007). Deformation in the presence of fluids and min-
1347 eral reactions effect of fracturing and fluid-rock interaction on seismic cycles.
1348 In (Vol. 95, p. 319-356).
- 1349 Greenberger, R. N., Mustard, J. F., Cloutis, E. A., Pratt, L. M., Sauer, P. E., Mann,
1350 P., ... Bish, D. L. (2015). Serpentinization, iron oxidation, and aqueous
1351 conditions in an ophiolite: Implications for hydrogen production and hab-
1352 itability on mars. *Earth and Planetary Science Letters*, 416, 21-34. doi:
1353 10.1016/j.epsl.2015.02.002
- 1354 Greening, C., Biswas, A., Carere, C. R., Jackson, C. J., Taylor, M. C., Stott, M. B.,
1355 ... Morales, S. E. (2016). Genomic and metagenomic surveys of hydrogenase
1356 distribution indicate h₂ is a widely utilised energy source for microbial growth
1357 and survival. *ISME Journal*, 10, 761-777. doi: 10.1038/ismej.2015.153
- 1358 Gregory, S. P., Barnett, M. J., Field, L. P., & Milodowski, A. E. (2019). Subsurface
1359 microbial hydrogen cycling: Natural occurrence and implications for industry.
1360 *Microorganisms*, 7. doi: 10.3390/microorganisms7020053
- 1361 Hancock, P. L., Chalmers, R. M. L., Altunel, E., & Cakir, Z. (1999). Traviton-
1362 ics: using travertines in active fault studies. *Journal of Structural Geology*, 21,
1363 903-916. Retrieved from www.elsevier.nl/locate/jstrugeo
- 1364 Hand, E. (2023). Hidden hydrogen: Does earth hold vast stores of a renewable,
1365 carbon-free fuel? *Science*, 379, 631-636.
- 1366 Hantschel, T., & Kauerauf, A. (2009). *Fundamentals of basin and petroleum systems*
1367 *modeling.* Springer.
- 1368 Harris, S. H., Smith, R. L., & Sufita, J. M. (2007). In situ hydrogen consump-
1369 tion kinetics as an indicator of subsurface microbial activity. *FEMS Microbiol-*
1370 *ogy Ecology*, 60, 220-228. doi: 10.1111/j.1574-6941.2007.00286.x
- 1371 Hemme, C., & van Berk, W. (2018). Hydrogeochemical modeling to identify poten-
1372 tial risks of underground hydrogen storage in depleted gas fields. *Applied Sci-*
1373 *ences (Switzerland)*, 8. doi: 10.3390/app8112282
- 1374 Hilton, D. R., Hammerschmidt, K., Looock, G., & Friedrichsen, H. (1993). He-
1375 lium and argon isotope systematics of the central lau basin and valu fa ridge:
1376 Evidence of crust/mantle interactions in a back-arc basin. *Geochimica et*
1377 *Cosmochimica Acta*, 57, 2819-2841.
- 1378 Holm, N. G., Oze, C., Mousis, O., Waite, J. H., & Guilbert-Lepoutre, A. (2015).
1379 Serpentinization and the formation of h₂ and ch₄ on celestial bodies (planets,
1380 moons, comets). *Astrobiology*, 15, 587-600. doi: 10.1089/ast.2014.1188
- 1381 Hopp, J., & Trieloff, M. (2008). Helium deficit in high-³He/⁴He parent magmas:
1382 Predegassing fractionation, not a "helium paradox". *Geochemistry, Geophysics,*
1383 *Geosystems*, 9. doi: 10.1029/2007GC001833
- 1384 Horsfield, B., Mahlstedt, N., Weniger, P., Misch, D., Vranjes-Wessely, S., Han, S.,
1385 & Wang, C. (2022). Molecular hydrogen from organic sources in the deep
1386 songliao basin, p.r. china. *International Journal of Hydrogen Energy*, 47,

- 1387 16750-16774. doi: 10.1016/j.ijhydene.2022.02.208
- 1388 Hosgörmez, H. (2007). Origin of the natural gas seep of Çirali (chimera), turkey:
- 1389 Site of the first olympic fire. *Journal of Asian Earth Sciences*, *30*, 131-141.
- 1390 doi: 10.1016/j.jseaes.2006.08.002
- 1391 Hoskin, C. M., & Sundeen, D. A. (1985). Grain size of granite and derived gres, en-
- 1392 chanted rock pluton, texas. *Sedimentary Geology*, *42*, 25-40.
- 1393 Hosseini, M., Fahimpour, J., Ali, M., Keshavarz, A., & Iglauer, S. (2022). H₂-brine
- 1394 interfacial tension as a function of salinity, temperature, and pressure; implica-
- 1395 tions for hydrogen geo-storage. *Journal of Petroleum Science and Engineering*,
- 1396 *213*. doi: 10.1016/j.petrol.2022.110441
- 1397 Huang, S., Lee, C. T. A., & Yin, Q. Z. (2014). Missing lead and high ³He/⁴He in an-
- 1398 cient sulfides associated with continental crust formation. *Scientific Reports*, *4*.
- 1399 doi: 10.1038/srep05314
- 1400 Hutchinson, I. P., Jackson, O., Stocks, A. E., Barnicoat, A. C., & Lawrence, S. R.
- 1401 (2024). Greenstones as a source of hydrogen in cratonic sedimentary basins.
- 1402 *Geological Society, London, Special Publications*, *547*. Retrieved from
- 1403 <https://www.lyellcollection.org/doi/10.1144/SP547-2023-39> doi:
- 1404 10.1144/SP547-2023-39
- 1405 Hydrogen, G. (2023). *Exploration update: Very high helium concentrations found*
- 1406 *at ramsay 2*. Retrieved from [https://www.goldhydrogen.com.au/wp/](https://www.goldhydrogen.com.au/wp/wp-content/uploads/2023.12.06-ASX-Announcement-Very-High-Helium-Concentrations-at-Ramsay-2.pdf)
- 1407 [wp-content/uploads/2023.12.06-ASX-Announcement-Very-High-Helium](https://www.goldhydrogen.com.au/wp/wp-content/uploads/2023.12.06-ASX-Announcement-Very-High-Helium-Concentrations-at-Ramsay-2.pdf)
- 1408 [-Concentrations-at-Ramsay-2.pdf](https://www.goldhydrogen.com.au/wp/wp-content/uploads/2023.12.06-ASX-Announcement-Very-High-Helium-Concentrations-at-Ramsay-2.pdf)
- 1409 IEA. (2021). *Global hydrogen review 2021*. Retrieved from [https://iea.blob](https://iea.blob.core.windows.net/assets/5bd46d7b-906a-4429-abda-e9c507a62341/GlobalHydrogenReview2021.pdf)
- 1410 [.core.windows.net/assets/5bd46d7b-906a-4429-abda-e9c507a62341/](https://iea.blob.core.windows.net/assets/5bd46d7b-906a-4429-abda-e9c507a62341/GlobalHydrogenReview2021.pdf)
- 1411 [GlobalHydrogenReview2021.pdf](https://iea.blob.core.windows.net/assets/5bd46d7b-906a-4429-abda-e9c507a62341/GlobalHydrogenReview2021.pdf)
- 1412 Iglauer, S., Mathew, M. S., & Bresme, F. (2012). Molecular dynamics computa-
- 1413 tions of brine-co₂ interfacial tensions and brine-co₂-quartz contact angles and
- 1414 their effects on structural and residual trapping mechanisms in carbon geo-
- 1415 sequestration. *Journal of Colloid and Interface Science*, *386*, 405-414. doi:
- 1416 10.1016/j.jcis.2012.06.052
- 1417 Ireland, M. T., Morley, C. K., & Davies, R. J. (2021). Systematic spacing and topo-
- 1418 logical variations in layer-bound fault systems. *Basin Research*, *33*, 2745-2762.
- 1419 doi: 10.1111/bre.12582
- 1420 Jackson, M. G., Konter, J. G., & Becker, T. W. (2017). Primordial helium en-
- 1421 trained by the hottest mantle plumes. *Nature*, *542*, 340-343. doi: 10.1038/
- 1422 nature21023
- 1423 Jacobs, E., Aertsens, M., Maes, N., Bruggeman, C., Krooss, B. M., Amann-
- 1424 Hildenbrand, A., ... Littke, R. (2017). Interplay of molecular size and pore
- 1425 network geometry on the diffusion of dissolved gases and hto in boom clay.
- 1426 *Applied Geochemistry*, *76*, 182-195. doi: 10.1016/j.apgeochem.2016.11.022
- 1427 Jimenez-Rodriguez, S., Quade, J., Levin, N. E., Campisano, C. J., Stinchcomb,
- 1428 G. E., Roman, D. C., & Bedaso, Z. (2023). Environmental controls on the
- 1429 hydrogen isotopic composition of volcanic glass from the southern afar rift,
- 1430 eastern ethiopia. *Chemical Geology*, *628*. doi: 10.1016/j.chemgeo.2023.121484
- 1431 Johnson, T. E., Brown, M., Gardiner, N. J., Kirkland, C. L., & Smithies, R. H.
- 1432 (2017). Earth's first stable continents did not form by subduction. *Nature*,
- 1433 *543*, 239-242. doi: 10.1038/nature21383
- 1434 Kalati, S. S., Khiabani, N. P., Ayatollahi, S., Mahani, H., Zivar, D., & Esmailbeig,
- 1435 M. A. (2024). Molecular dynamics simulation of hydrogen diffusion into
- 1436 brine: Implications for underground hydrogen storage. *International Journal of*
- 1437 *Hydrogen Energy*, *53*, 17-28. doi: 10.1016/j.ijhydene.2023.11.318
- 1438 Kampman, N., Burnside, N. M., Shipton, Z. K., Chapman, H. J., Nicholl, J. A., El-
- 1439 lam, R. M., & Bickle, M. J. (2012). Pulses of carbon dioxide emissions from
- 1440 intracrustal faults following climatic warming. *Nature Geoscience*, *5*, 352-358.
- 1441 doi: 10.1038/ngeo1451

- 1442 Karato, S. (2007). Microscopic models for the effects of hydrogen on physical and
 1443 chemical properties of earth materials. In D. Yuen, S. Maruyama, S. Karato, &
 1444 B. Windley (Eds.), (p. 321-351). Springer.
- 1445 Karolyt , R., Warr, O., van Heerden, E., Flude, S., de Lange, F., Webb, S., . . . Lol-
 1446 lar, B. S. (2022). The role of porosity in h₂/he production ratios in fracture
 1447 fluids from the witwatersrand basin, south africa. *Chemical Geology*, *595*. doi:
 1448 10.1016/j.chemgeo.2022.120788
- 1449 Kellogg, L. H., & Wasserburg, G. J. (1990). *The role of plumes in mantle helium*
 1450 *fluxes*. Elsevier Science Publishers B.V.
- 1451 Keshavarz, A., Abid, H., Ali, M., & Iglauer, S. (2022). Hydrogen diffusion in coal:
 1452 Implications for hydrogen geo-storage. *Journal of Colloid and Interface Sci-*
 1453 *ence*, *608*, 1457-1462. doi: 10.1016/j.jcis.2021.10.050
- 1454 Klein, F., Bach, W., & McCollom, T. M. (2013). Compositional controls on hydro-
 1455 gen generation during serpentinization of ultramafic rocks. *Lithos*, *178*, 55-69.
 1456 doi: 10.1016/j.lithos.2013.03.008
- 1457 Kohlstedt, D., & Mackwell, S. (1998). Diffusion of hydrogen and intrinsic point de-
 1458 fects in olivine. *Zeitschrift f r physikalische Chemie*, *207*, 147-162.
- 1459 Koproch, N., Dahmke, A., & K ber, R. (2019). The aqueous solubility of common
 1460 organic groundwater contaminants as a function of temperature between 5 and
 1461 70 c. *Chemosphere*, *217*, 166-175. doi: 10.1016/j.chemosphere.2018.10.153
- 1462 Kotelnikova, S., & Pedersen, K. (1998). Distribution and activity of methanogens
 1463 and homoacetogens in deep granitic aquifers at aspo hard rock labora-
 1464 tory, sweden. *FEMS Microbiology Ecology*, *26*, 121-134. doi: 10.1111/
 1465 j.1574-6941.1998.tb00498.x
- 1466 Kufner, S. K., Kakar, N., Bezada, M., Bloch, W., Metzger, S., Yuan, X., . . .
 1467 Schurr, B. (2021). The hindu kush slab break-off as revealed by deep
 1468 structure and crustal deformation. *Nature Communications*, *12*. doi:
 1469 10.1038/s41467-021-21760-w
- 1470 Kurz, M. D., Jenkins, W. J., & Hart, S. R. (1982). *Helium isotopic systematics of*
 1471 *oceanic islands and mantle heterogeneity* (Vol. 297).
- 1472 Lamadrid, H. M., Rimstidt, J. D., Schwarzenbach, E. M., Klein, F., Ulrich, S., Dolo-
 1473 can, A., & Bodnar, R. J. (2017). Effect of water activity on rates of serpen-
 1474 tinization of olivine. *Nature Communications*, *8*. doi: 10.1038/ncomms16107
- 1475 Lefevre, N., Thomas, E., Truche, L., Donz , F., Cros, T., Dupuy, J., . . . Rigollet,
 1476 C. (2024, 5). Characterizing natural hydrogen occurrences in the paris basin
 1477 from historical drilling records. *Geochemistry, Geophysics, Geosystems*, *25*.
 1478 Retrieved from [https://agupubs.onlinelibrary.wiley.com/doi/10.1029/](https://agupubs.onlinelibrary.wiley.com/doi/10.1029/2024GC011501)
 1479 [2024GC011501](https://agupubs.onlinelibrary.wiley.com/doi/10.1029/2024GC011501) doi: 10.1029/2024GC011501
- 1480 Lefevre, N., Truche, L., Donz , F. V., Ducoux, M., Barr , G., Fakoury, R. A.,
 1481 . . . Gaucher, E. C. (2021). Native h₂ exploration in the western pyre-
 1482 nean foothills. *Geochemistry, Geophysics, Geosystems*, *22*, 1-20. doi:
 1483 10.1029/2021GC009917
- 1484 Lefevre, N., Truche, L., Donz , F. V., Gal, F., Tremosa, J., Fakoury, R. A., . . .
 1485 Gaucher, E. C. (2022). Natural hydrogen migration along thrust faults in
 1486 foothill basins: The north pyrenean frontal thrust case study. *Applied Geo-*
 1487 *chemistry*, *145*. doi: 10.1016/j.apgeochem.2022.105396
- 1488 Li, J., & Chou, I. M. (2015). Hydrogen in silicate melt inclusions in quartz from
 1489 granite detected with raman spectroscopy. *Journal of Raman Spectroscopy*, *46*,
 1490 983-986. doi: 10.1002/jrs.4644
- 1491 Lin, L. H., Slater, G. F., Lollar, B. S., Lacrampe-Couloume, G., & Onstott, T. C.
 1492 (2005). The yield and isotopic composition of radiolytic h₂, a potential energy
 1493 source for the deep subsurface biosphere. *Geochimica et Cosmochimica Acta*,
 1494 *69*, 893-903. doi: 10.1016/j.gca.2004.07.032
- 1495 Lin, S. C., & Keken, P. E. V. (2006). Dynamics of thermochemical plumes: 1.
 1496 plume formation and entrainment of a dense layer. *Geochemistry, Geophysics,*

- 1497 *Geosystems*, 7. doi: 10.1029/2005GC001071
- 1498 Lis, D. C., Bockelée-Morvan, D., Güsten, R., Biver, N., Stutzki, J., Delorme,
1499 Y., ... Okada, Y. (2019). Terrestrial deuterium-to-hydrogen ratio in
1500 water in hyperactive comets. *Astronomy and Astrophysics*, 625. doi:
1501 10.1051/0004-6361/201935554
- 1502 Liu, J., Wang, S., Javadpour, F., Feng, Q., & Cha, L. (2022). Hydrogen diffusion in
1503 clay slit: Implications for the geological storage. *Energy and Fuels*, 36, 7651-
1504 7660. doi: 10.1021/acs.energyfuels.2c01189
- 1505 Liu, Z., Perez-Gussinye, M., García-Pintado, J., Mezri, L., & Bach, W. (2023). Man-
1506 tle serpentinization and associated hydrogen flux at north atlantic magma-poor
1507 rifted margins. *Geology*, 51, 284-289. doi: 10.1130/G50722.1
- 1508 Lodhia, B. H. (2023). *hydrogen_mobility (version 1.0.0) [software]*. doi: 10.5281/
1509 zenodo.10990920
- 1510 Lodhia, B. H., & Clark, S. R. (2022). Computation of vertical fluid mobility of co2
1511 , methane , hydrogen and hydrocarbons through sandstones and carbonates.
1512 *Scientific Reports*, 1-14. doi: 10.1038/s41598-022-14234-6
- 1513 Lodhia, B. H., & Peeters, L. (2024). The migration of hydrogen in sedimentary
1514 basins. *Australian Energy Producers Journal*, 64, 186-194. doi:
1515 10.1071/EP23176
- 1516 Loewen, M. W., Graham, D. W., Bindeman, I. N., Lupton, J. E., & Garcia, M. O.
1517 (2019). Hydrogen isotopes in high 3 he/ 4 he submarine basalts: Primordial vs.
1518 recycled water and the veil of mantle enrichment. *Earth and Planetary Science*
1519 *Letters*, 508, 62-73. doi: 10.1016/j.epsl.2018.12.012
- 1520 Lollar, B. S., Onstott, T. C., Lacrampe-Couloume, G., & Ballentine, C. J. (2014).
1521 The contribution of the precambrian continental lithosphere to global h2 pro-
1522 duction. *Nature*, 516, 379-382. doi: 10.1038/nature14017
- 1523 Lopez-Lazaro, C., Bachaud, P., Moretti, I., & Ferrando, N. (2019). Predict-
1524 ing the phase behavior of hydrogen in nacl brines by molecular simulation
1525 for geological applications. *BSGF - Earth Sciences Bulletin*, 190. doi:
1526 10.1051/bsgf/2019008
- 1527 Lupton, J., & Craig, H. (1975). Excess 3he in oceanic basalts: Evidence for terres-
1528 trial primordial helium. *Earth and Planetary Science Letters*, 26, 133-139. doi:
1529 https://doi.org/10.1016/0012-821x(75)90080-1
- 1530 Lévy, D., Boka-Mene, M., Meshi, A., Fejza, I., Guermont, T., Hauville, B., &
1531 Pelissier, N. (2023). Looking for natural hydrogen in albania and kosova.
1532 *Frontiers in Earth Science*, 11. doi: 10.3389/feart.2023.1167634
- 1533 Lévy, D., Roche, V., Pasquet, G., Combaudon, V., Geymond, U., Loiseau, K., &
1534 Moretti, I. (2023). Natural h2 exploration: tools and workflows to character-
1535 ize a play. *Science and Technology for Energy Transition (STET)*, 78. doi:
1536 10.2516/stet/2023021
- 1537 Mackintosh, S. J., & Ballentine, C. J. (2012). Using 3he/ 4he isotope ratios to iden-
1538 tify the source of deep reservoir contributions to shallow fluids and soil gas.
1539 *Chemical Geology*, 304-305, 142-150. doi: 10.1016/j.chemgeo.2012.02.006
- 1540 Magnabosco, C., Lin, L. H., Dong, H., Bomberg, M., Ghiorse, W., Stan-Lotter, H.,
1541 ... Onstott, T. C. (2018). *The biomass and biodiversity of the continental sub-*
1542 *surface* (Vol. 11). Nature Publishing Group. doi: 10.1038/s41561-018-0221-6
- 1543 Mahlstedt, N., Horsfield, B., Weniger, P., Misch, D., Shi, X., Noah, M., & Bore-
1544 ham, C. (2022). Molecular hydrogen from organic sources in geologi-
1545 cal systems. *Journal of Natural Gas Science and Engineering*, 105. doi:
1546 10.1016/j.jngse.2022.104704
- 1547 Mangenot, X., Xie, H., Crémière, A., Giunta, T., Lilley, M., Sissmann, O., ... Eiler,
1548 J. (2023). 2h-2h clumping in molecular hydrogen method and preliminary
1549 results. *Chemical Geology*, 621. doi: 10.1016/j.chemgeo.2022.121278
- 1550 Marcaillou, C., Muñoz, M., Vidal, O., Parra, T., & Harfouche, M. (2011). Min-
1551 eralogical evidence for h2 degassing during serpentinization at 300°C/300bar.

- 1552 *Earth and Planetary Science Letters*, *303*, 281-290. doi: 10.1016/j.epsl.2011.01
1553 .006
- 1554 Marques, J. M., Etiope, G., Neves, M. O., Carreira, P. M., Rocha, C., Vance,
1555 S. D., ... Suzuki, S. (2018). Linking serpentinization, hyperalkaline min-
1556 eral waters and abiotic methane production in continental peridotites: an
1557 integrated hydrogeological-bio-geochemical model from the cabeço de vide
1558 ch4-rich aquifer (portugal). *Applied Geochemistry*, *96*, 287-301. doi:
1559 10.1016/j.apgeochem.2018.07.011
- 1560 Marty, B. (2012). The origins and concentrations of water, carbon, nitrogen and no-
1561 ble gases on earth. *Earth and Planetary Science Letters*, *313-314*, 56-66. doi:
1562 10.1016/j.epsl.2011.10.040
- 1563 Marty, B., & Yokochi, R. (2006). Water in the early earth. *Reviews in Mineralogy &
1564 Geochemistry*, *62*, 421-450. doi: 10.2138/rmg.2006.62.18
- 1565 Massiot, C., Seebeck, H., Nicol, A., McNamara, D. D., Lawrence, M. J., Griffin,
1566 A. G., ... Viskovic, G. P. D. (2019). Effects of regional and local stresses on
1567 fault slip tendency in the southern taranaki basin, new zealand. *Marine and
1568 Petroleum Geology*, *107*, 467-483. doi: 10.1016/j.marpetgeo.2019.05.030
- 1569 Mathiesen, J., Linga, G., Misztal, M., Renard, F., & Borgne, T. L. (2023). Dynamic
1570 fluid connectivity controls solute dispersion in multiphase porous media flow.
1571 *Geophysical Research Letters*, *50*. doi: 10.1029/2023GL105233
- 1572 McCollom, T. M., & Amend, J. P. (2005). A thermodynamic assessment of en-
1573 ergy requirements for biomass synthesis by chemolithoautotrophic micro-
1574 organisms in oxic and anoxic environments. *Geobiology*, *3*, 135-144. doi:
1575 10.1111/j.1472-4669.2005.00045.x
- 1576 Moretti, I., Brouilly, E., Loiseau, K., Prinzhofer, A., & Deville, E. (2021). Hydrogen
1577 emanations in intracratonic areas: New guide lines for early exploration basin
1578 screening. *Geosciences*, *11*. doi: 10.3390/geosciences11030145
- 1579 Moretti, I., Prinzhofer, A., Françolin, J., Pacheco, C., Rosanne, M., Rupin, F., &
1580 Mertens, J. (2021). Long-term monitoring of natural hydrogen superficial
1581 emissions in a brazilian cratonic environment. sporadic large pulses versus
1582 daily periodic emissions. *International Journal of Hydrogen Energy*, *46*, 3615-
1583 3628. doi: 10.1016/j.ijhydene.2020.11.026
- 1584 Morgan, W. (1971). Convection plumes in the lower mantle. *Nature*, *230*, 42-43.
- 1585 Mostinsky, I. L. (2011). Diffusion coefficient. Begellhouse. doi: 10.1615/AtoZ.d
1586 .diffusion_coefficient
- 1587 Muhammed, N. S., Haq, B., Shehri, D. A., Al-Ahmed, A., Rahman, M. M., & Za-
1588 man, E. (2022). A review on underground hydrogen storage: Insight into
1589 geological sites, influencing factors and future outlook. *Energy Reports*, *8*,
1590 461-499. doi: 10.1016/j.egy.2021.12.002
- 1591 Mukhopadhyay, S. (2012). Early differentiation and volatile accretion recorded
1592 in deep-mantle neon and xenon. *Nature*, *486*, 101-104. doi: 10.1038/
1593 nature11141
- 1594 Myagkiy, A., Brunet, F., Popov, C., Krüger, R., Guimarães, H., Sousa, R. S., ...
1595 Moretti, I. (2020). H2 dynamics in the soil of a h2-emitting zone (são francisco
1596 basin, brazil): Microbial uptake quantification and reactive transport mod-
1597 elling. *Applied Geochemistry*, *112*. doi: 10.1016/j.apgeochem.2019.104474
- 1598 Myagkiy, A., Moretti, I., & Brunet, F. (2020). Space and time distribution of
1599 subsurface h2concentration in so-called "fairy circles": Insight from a con-
1600 ceptual 2-d transport model. *BSGF - Earth Sciences Bulletin*, *191*. doi:
1601 10.1051/bsgf/2020010
- 1602 Nealson, K. H., Inagaki, F., & Takai, K. (2005). Hydrogen-driven subsurface
1603 lithoautotrophic microbial ecosystems (slimes): Do they exist and why should
1604 we care? *Trends in Microbiology*, *13*, 405-410. doi: 10.1016/j.tim.2005.07.010
- 1605 Neelamegham, N. R., Subramanian, G., & Kalamegham, P. (2022). Thermoeco-
1606 nomic dynamics of energy-efficient orange hydrogen production: An energy

- 1607 matter. *JOM*, 74, 1923-1931. doi: 10.1007/s11837-022-05162-x
- 1608 Nestola, F., & Smyth, J. R. (2016). *Diamonds and water in the deep earth: A*
 1609 *new scenario* (Vol. 58). Taylor and Francis Inc. doi: 10.1080/00206814.2015
 1610 .1056758
- 1611 Niwa, M., Kurosawa, H., Shimada, K., Ishimaru, T., & Kosaka, H. (2011). Identifi-
 1612 cation of pathways for hydrogen gas migration in fault zones with a discontinu-
 1613 ous, heterogeneous permeability structure and the relationship to particle size
 1614 distribution of fault materials. *Pure and Applied Geophysics*, 168, 887-900.
 1615 doi: 10.1007/s00024-010-0167-0
- 1616 Nova, A., Prifti, K., Negri, F., & Manenti, F. (2023). Multiscale techno-economic
 1617 analysis of orange hydrogen synthesis. *Energy*, 282. doi: 10.1016/j.energy.2023
 1618 .128644
- 1619 of Energy, U. D. (2024). *U.s. department of energy announces \$20 million*
 1620 *to 16 projects spearheading exploration of geologic hydrogen*. Retrieved
 1621 from [https://arpa-e.energy.gov/news-and-media/press-releases/us](https://arpa-e.energy.gov/news-and-media/press-releases/us-department-energy-announces-20-million-16-projects-spearheading)
 1622 [-department-energy-announces-20-million-16-projects-spearheading](https://arpa-e.energy.gov/news-and-media/press-releases/us-department-energy-announces-20-million-16-projects-spearheading)
- 1623 O'hanley, D. S. (1992). Solution to the volume problem in serpentinization. *Ge-*
 1624 *ology*, 20, 705-708. Retrieved from [http://pubs.geoscienceworld.org/gsa/](http://pubs.geoscienceworld.org/gsa/geology/article-pdf/20/8/705/3513947/i0091-7613-20-8-705.pdf)
 1625 [geology/article-pdf/20/8/705/3513947/i0091-7613-20-8-705.pdf](http://pubs.geoscienceworld.org/gsa/geology/article-pdf/20/8/705/3513947/i0091-7613-20-8-705.pdf)
- 1626 Olson, P. L., & Sharp, Z. D. (2022). Primordial helium-3 exchange between earth's
 1627 core and mantle. *Geochemistry, Geophysics, Geosystems*, 23. doi: 10.1029/
 1628 2021GC009985
- 1629 Osselin, F., Pichavant, M., Champallier, R., Ulrich, M., & Raimbourg, H. (2022).
 1630 Reactive transport experiments of coupled carbonation and serpentinization
 1631 in a natural serpentinite. implication for hydrogen production and carbon
 1632 geological storage. *Geochimica et Cosmochimica Acta*, 318, 165-189. doi:
 1633 10.1016/j.gca.2021.11.039
- 1634 Owczarek, E., & Zakroczymski, T. (2000). Hydrogen transport in a duplex stainless
 1635 steel. *Acta mater*, 48, 3059-3070. Retrieved from [www.elsevier.com/locate/](http://www.elsevier.com/locate/actamat)
 1636 [actamat](http://www.elsevier.com/locate/actamat)
- 1637 Parnell, J., & Blamey, N. (2017). Global hydrogen reservoirs in basement and
 1638 basins. *Geochemical Transactions*, 18. doi: 10.1186/s12932-017-0041-4
- 1639 Perchuk, A. L., Zakharov, V. S., Gerya, T. V., & Griffin, W. L. (2023). Flat subduc-
 1640 tion in the early earth: The key role of discrete eclogitization kinetics. *Gond-*
 1641 *wana Research*, 119, 186-203. doi: 10.1016/j.gr.2023.03.015
- 1642 Peslier, A. H., & Bizimis, M. (2015). Water in hawaiian peridotite minerals: A
 1643 case for a dry metasomatized oceanic mantle lithosphere. *Geochemistry, Geo-*
 1644 *physics, Geosystems*, 16, 1211-1232. doi: 10.1002/2015GC005780
- 1645 Peslier, A. H., Schönbächler, M., Busemann, H., & Karato, S. I. (2017). Water in
 1646 the earth's interior: Distribution and origin. *Space Science Reviews*, 212, 743-
 1647 810. doi: 10.1007/s11214-017-0387-z
- 1648 Pinti, D. L. (2021). Deuterium/hydrogen ratio. in: , et al. In (p. 1-3). Re-
 1649 trieved from [https://link.springer.com/referenceworkentry/10.1007/](https://link.springer.com/referenceworkentry/10.1007/978-3-642-278...)
 1650 [978-3-642-278...](https://link.springer.com/referenceworkentry/10.1007/978-3-642-278...) doi: 10.1007/978-3-642-278
- 1651 Polat, A., & Hofmann, A. W. (2003). Alteration and geochemical patterns in the
 1652 3.7-3.8 ga isua greenstone belt, west greenland. In (Vol. 126, p. 197-218). Else-
 1653 vier B.V. doi: 10.1016/S0301-9268(03)00095-0
- 1654 Porcelli, D., & Elliott, T. (2008, 5). The evolution of he isotopes in the convecting
 1655 mantle and the preservation of high 3he/4he ratios. *Earth and Planetary Sci-*
 1656 *ence Letters*, 269, 175-185. doi: 10.1016/j.epsl.2008.02.002
- 1657 Poreda, R., Schilling, J.-G., & Craig, H. (1986). Helium and hydrogen isotopes
 1658 in ocean-ridge basalts north and south of iceland. *Earth and Planetary Science*
 1659 *Letters*, 78, 1-17. doi: [https://doi.org/10.1016/0012-821X\(86\)90168-8](https://doi.org/10.1016/0012-821X(86)90168-8)
- 1660 Prinzhofer, A., & Cacas-Stentz, M. C. (2023). Natural hydrogen and blend gas:
 1661 a dynamic model of accumulation. *International Journal of Hydrogen Energy*,

- 1662 48, 21610-21623. doi: 10.1016/j.ijhydene.2023.03.060
- 1663 Prinzhofer, A., Cissé, C. S. T., & Diallo, A. B. (2018). Discovery of a large accumu-
 1664 lation of natural hydrogen in bourakebougou (mali). *International Journal of*
 1665 *Hydrogen Energy*, 43, 19315-19326. doi: 10.1016/j.ijhydene.2018.08.193
- 1666 Prinzhofer, A., Moretti, I., Françolin, J., Pacheco, C., D'Agostino, A., Werly, J., &
 1667 Rupin, F. (2019). Natural hydrogen continuous emission from sedimentary
 1668 basins: The example of a brazilian h₂-emitting structure. *International Jour-*
 1669 *nal of Hydrogen Energy*, 44, 5676-5685. doi: 10.1016/j.ijhydene.2019.01.119
- 1670 Renard, F., Candela, T., & Bouchaud, E. (2013). Constant dimensionality of fault
 1671 roughness from the scale of micro-fractures to the scale of continents. *Geophys-*
 1672 *ical Research Letters*, 40, 83-87. doi: 10.1029/2012GL054143
- 1673 Rezaee, R. (2021). Assessment of natural hydrogen systems in western aus-
 1674 tralia. *International Journal of Hydrogen Energy*, 46, 33068-33077. doi:
 1675 10.1016/j.ijhydene.2021.07.149
- 1676 Rhode, M., Richter, T., Mente, T., Mayr, P., & Nitsche, A. (2022). Thickness
 1677 and microstructure effect on hydrogen diffusion in creep-resistant 9 % cr
 1678 p92 steel and p91 weld metal. *Welding in the World*, 66, 325-340. doi:
 1679 10.1007/s40194-021-01218-9
- 1680 Rison, W., & Craig, H. (1983). *Helium isotopes and mantle volatiles in loihi*
 1681 *seamount and hawaiian island basalts and xenoliths* (Vol. 66).
- 1682 Roden, E. E., & Jin, Q. (2011, 3). Thermodynamics of microbial growth cou-
 1683 pled to metabolism of glucose, ethanol, short-chain organic acids, and hy-
 1684 drogen. *Applied and Environmental Microbiology*, 77, 1907-1909. doi:
 1685 10.1128/AEM.02425-10
- 1686 Rouméjon, S., & Cannat, M. (2014). Serpentinization of mantle-derived peridotites
 1687 at mid-ocean ridges: Mesh texture development in the context of tectonic
 1688 exhumation. *Geochemistry, Geophysics, Geosystems*, 15, 2354-2379. doi:
 1689 10.1002/2013GC005148
- 1690 Roy, S., Raju, R., Chuang, H. F., Cruden, B. A., & Meyyappan, M. (2003). Mod-
 1691 eling gas flow through microchannels and nanopores. *Journal of Applied*
 1692 *Physics*, 93, 4870-4879. doi: 10.1063/1.1559936
- 1693 Sakhaee-Pour, A., & Alessa, S. (2022). Hydrogen permeability in subsurface. *Inter-*
 1694 *national Journal of Hydrogen Energy*, 47, 27071-27079. doi: 10.1016/j.ijhydene
 1695 .2022.06.042
- 1696 Salerno, E., Bühler, F., Bochsler, P., Busemann, H., Bassi, M., Zastenker, G., ...
 1697 Eismont, N. (2003). Measurement of 3he/4he in the local interstellar medium:
 1698 The collisa experiment on mir. *The Astrophysical Journal*, 585, 840.
- 1699 Samuel, H., & Farnetani, C. G. (2003). Thermochemical convection and helium con-
 1700 centrations in mantle plumes. *Earth and Planetary Science Letters*, 207, 39-56.
 1701 doi: 10.1016/S0012-821X(02)01125-1
- 1702 Sano, Y., Urabe, A., & Wakita, H. (1993). Origin of hydrogen-nitrogen gas seeps,
 1703 oman hisao wushiki . *Applied Geochemistry*, 8, 1-8.
- 1704 Schink, B., Thiemann, V., Laue, H., & Friedrich, M. W. (2002). Desul-
 1705 fotignum phosphitoxidans sp. nov., a new marine sulfate reducer that oxi-
 1706 dizes phosphite to phosphate. *Archives of Microbiology*, 177, 381-391. doi:
 1707 10.1007/s00203-002-0402-x
- 1708 Schlinger, C. M., Rosenbaum, J. G., & Veblen, D. R. (1988). Fe-oxide micro-
 1709 crystals in welded tuff from southern nevada: Origin of remanence carriers
 1710 by precipitation in volcanic glass. *Geology*, 16, 556-559. Retrieved from
 1711 [http://pubs.geoscienceworld.org/gsa/geology/article-pdf/16/6/556/
 1712 3510934/i0091-7613-16-6-556.pdf](http://pubs.geoscienceworld.org/gsa/geology/article-pdf/16/6/556/3510934/i0091-7613-16-6-556.pdf)
- 1713 Seton, M., Müller, R. D., Zahirovic, S., Williams, S. E., Nicky, M. W., Cannon, J.,
 1714 ... McGirr, R. (2020). A global data set of present-day oceanic crustal age
 1715 and seafloor spreading parameters. *Geochemistry, Geophysics, Geosystems*, 21.
 1716 doi: 10.1029/2020GC009214

- 1717 Sharapov, V., Semenov, Y., Kuznetsov, G., & Boguslavsky, A. (2022). Spinel crystals
1718 in mantle ultramafic xenoliths as the source of p-t conditions of alteration
1719 above the magma chamber beneath the avacha volcano (kamchatka). *Journal*
1720 *of Asian Earth Sciences: X*, 8. doi: 10.1016/j.jaesx.2022.100119
- 1721 Shaw, A. M., Hauri, E. H., Fischer, T. P., Hilton, D. R., & Kelley, K. A. (2008).
1722 Hydrogen isotopes in mariana arc melt inclusions: Implications for subduction
1723 dehydration and the deep-earth water cycle. *Earth and Planetary Science*
1724 *Letters*, 275, 138-145. doi: 10.1016/j.epsl.2008.08.015
- 1725 Shirey, S., & S.H., R. (2011). Start of the wilson cycle at 3 ga shown by dia-
1726 monds from subcontinental mantle. *Science*, 333, 434-436. doi: 10.1126/
1727 science.1204255
- 1728 Smithies, R. H., Champion, D. C., & Cassidy, K. F. (2003). Formation of earth's
1729 early archaean continental crust. *Precambrian Research*, 127, 89-101. doi: 10
1730 .1016/S0301-9268(03)00182-7
- 1731 Solomatov, V. S., & Moresi, L. N. (2000). Scaling of time-dependent stagnant lid
1732 convection: Application to small-scale convection on earth and other terrestrial
1733 planets. *Journal of Geophysical Research: Solid Earth*, 105, 21795-21817. doi:
1734 10.1029/2000jb900197
- 1735 Solum, J. G., Davatzes, N. C., & Lockner, D. A. (2010). Fault-related clay au-
1736 thigenesis along the moab fault: Implications for calculations of fault rock
1737 composition and mechanical and hydrologic fault zone properties. *Journal of*
1738 *Structural Geology*, 32, 1899-1911. doi: 10.1016/j.jsg.2010.07.009
- 1739 Speciale, P. A., Behr, W. M., Hirth, G., & Tokle, L. (2020). Rates of olivine grain
1740 growth during dynamic recrystallization and postdeformation annealing. *Jour-*
1741 *nal of Geophysical Research: Solid Earth*, 125. doi: 10.1029/2020JB020415
- 1742 Sperner, B., Lorenz, F., Bonjer, K., Hettel, S., Müller, B., & Wenzel, F. (2001).
1743 Slab break-off - abrupt cut or gradual detachment? new insights from the
1744 vrancea region (se carpathians, romania). *Terra Nova*, 13, 172-179. doi:
1745 10.1046/j.1365-3121.2001.00335.x
- 1746 Stevens, T. O., & McKinley, J. P. (2000). Abiotic controls on h2 production from
1747 basalt - water reactions and implications for aquifer biogeochemistry. *Environ-*
1748 *mental Science and Technology*, 34, 826-831. doi: 10.1021/es990583g
- 1749 Strauch, B., Pilz, P., Hierold, J., & Zimmer, M. (2023). Experimental simulations of
1750 hydrogen migration through potential storage rocks. *International Journal of*
1751 *Hydrogen Energy*, 48, 25808-25820. doi: 10.1016/j.ijhydene.2023.03.115
- 1752 Su, Q., Zeller, E., & Angino, E. (1992). Inducing action of hydrogen migrating along
1753 faults on earthquakes. *Acta Seismologica Sinica*, 5, 841-847. doi: 10.1007/
1754 BF02651032
- 1755 Takai, K., Gamo, T., Tsunogai, U., Nakayama, N., Hirayama, H., Nealson, K. H.,
1756 & Horikoshi, K. (2004). Geochemical and microbiological evidence for a
1757 hydrogen-based, hyperthermophilic subsurface lithoautotrophic microbial
1758 ecosystem (hyperslime) beneath an active deep-sea hydrothermal field. *Ex-*
1759 *tremophiles*, 8, 269-282. doi: 10.1007/s00792-004-0386-3
- 1760 Templeton, A. S., Ellison, E. T., Kelemen, P. B., Leong, J., Boyd, E. S., Colman,
1761 D. R., & Matter, J. M. (2024). Low-temperature hydrogen production
1762 and consumption in partially-hydrated peridotites in oman: implications
1763 for stimulated geological hydrogen production. *Frontiers in Geochemistry*,
1764 2. Retrieved from [https://www.frontiersin.org/articles/10.3389/
1765 fgeoc.2024.1366268/full](https://www.frontiersin.org/articles/10.3389/fgeoc.2024.1366268/full) doi: 10.3389/fgeoc.2024.1366268
- 1766 Thauer, R. K., Jungermann, K., & Decker, K. (1977). Energy conservation in
1767 chemotrophic anaerobic bacteria. *Bacteriological Reviews*, 41, 100-180. Re-
1768 trieved from <https://journals.asm.org/journal/br>
- 1769 ToolBox, E. (2018). *Air - diffusion coefficients of gases in excess of air*.
- 1770 Torres, M. E. S., Saucedo-Vázquez, J. P., & Kroneck, P. M. H. (2015). The magic of
1771 dioxygen. In M. S. Torres (Ed.), (Vol. 15, p. 1-12). Springer. doi: 10.1007/978

- 1772 -3-319-12415-5_1
- 1773 Truche, L., Donzé, F.-V., Guskolli, E., Muceku, B., Loisy, C., Monnin, C., ...
- 1774 Cerepi, A. (2024). A deep reservoir for hydrogen drives intense de-
- 1775 gassing in the bulqizë ophiolite. *Science*, *383*, 618-621. Retrieved from
- 1776 <https://www.science.org> doi: 10.1126/science.adk9099
- 1777 Truche, L., Joubert, G., Dargent, M., Martz, P., Cathelineau, M., Rigaudier, T., &
- 1778 Qurt, D. (2018, 7). Clay minerals trap hydrogen in the earth's crust: Evidence
- 1779 from the cigar lake uranium deposit, athabasca. *Earth and Planetary Science*
- 1780 *Letters*, *493*, 186-197. doi: 10.1016/j.epsl.2018.04.038
- 1781 Vacquand, C., Deville, E., Beaumont, V., Guyot, F., Sissmann, O., Pillot, D., ...
- 1782 Prinzhofer, A. (2018). Reduced gas seepages in ophiolitic complexes: Ev-
- 1783 idences for multiple origins of the h₂-ch₄-n₂ gas mixtures. *Geochimica et*
- 1784 *Cosmochimica Acta*, *223*, 437-461. doi: 10.1016/j.gca.2017.12.018
- 1785 van der Meer, D. G., van Hinsbergen, D. J., & Spakman, W. (2018). Atlas of
- 1786 the underworld: Slab remnants in the mantle, their sinking history, and a
- 1787 new outlook on lower mantle viscosity. *Tectonophysics*, *723*, 309-448. doi:
- 1788 10.1016/j.tecto.2017.10.004
- 1789 van Hunen, J., & van den Berg, A. P. (2008). Plate tectonics on the early earth:
- 1790 Limitations imposed by strength and buoyancy of subducted lithosphere.
- 1791 *Lithos*, *103*, 217-235. doi: 10.1016/j.lithos.2007.09.016
- 1792 Vinsot, A., Appelo, C. A., Lundy, M., Wechner, S., Lettry, Y., Lerouge, C., ... De-
- 1793 lay, J. (2014). In situ diffusion test of hydrogen gas in the opalinus clay.
- 1794 *Geological Society Special Publication*, *400*, 563-578. doi: 10.1144/SP400.12
- 1795 Wakita, H., Nakamura, Y., Kita, I., Fujii, N., & Notsu, K. (1980). Hydrogen re-
- 1796 lease: New indicator of fault activity. *Science*, *210*, 188-190. Retrieved from
- 1797 <https://www.science.org>
- 1798 Wan, B., Yang, X., Tian, X., Yuan, H., Kirscher, U., & Mitchell, R. N. (2020).
- 1799 *Seismological evidence for the earliest global subduction network at 2 ga ago*
- 1800 (Vol. 6). Retrieved from <https://www.science.org>
- 1801 Wang, C., Zhao, Y., Wu, R., Bi, J., & Zhang, K. (2024). Shale reservoir storage of
- 1802 hydrogen: Adsorption and diffusion on shale. *Fuel*, *357*. doi: 10.1016/j.fuel
- 1803 .2023.129919
- 1804 Wang, L., Cheng, J., Jin, Z., Sun, Q., Zou, R., Meng, Q., ... Zhang, Q. (2023).
- 1805 High-pressure hydrogen adsorption in clay minerals: Insights on natural hydro-
- 1806 gen exploration. *Fuel*, *344*. doi: 10.1016/j.fuel.2023.127919
- 1807 Wang, L., Jin, Z., Chen, X., Su, Y., & Huang, X. (2023). The origin and occurrence
- 1808 of natural hydrogen. *Energies*, *16*. doi: 10.3390/en16052400
- 1809 Wang, Z., & Becker, H. (2013). Ratios of s, se and te in the silicate earth require a
- 1810 volatile-rich late veneer. *Nature*, *499*, 328-331. doi: 10.1038/nature12285
- 1811 Williams, Q., & Hemley, R. J. (2001). Hydrogen in the deep earth. *An-*
- 1812 *nuual Review Earth Planetary Sciences*, *29*, 365-418. Retrieved from
- 1813 www.annualreviews.org
- 1814 Xia, Y., Yang, J., Chen, Y., Lu, S., Wang, M., Deng, S., ... Lu, M. (2022). A
- 1815 review of the global polygonal faults: Are they playing a big role in fluid mi-
- 1816 gration? *Frontiers in Earth Science*, *9*. doi: 10.3389/feart.2021.786915
- 1817 Yeo, B. (2023). *Why make what you can mine? here's why natural hydrogen is*
- 1818 *also known as 'gold' hydrogen*. Retrieved from [https://stockhead.com.au/energy/why-make-what-you-can-mine-heres-why-natural-hydrogen-is-also-known-as-gold-hydrogen/#:~:text=Gold%20Hydrogen%20\(ASX%3AGHY\)&text=The%20bulk%20of%20the%20remaining,drilled%20almost%20a%20century%20ago](https://stockhead.com.au/energy/why-make-what-you-can-mine-heres-why-natural-hydrogen-is-also-known-as-gold-hydrogen/#:~:text=Gold%20Hydrogen%20(ASX%3AGHY)&text=The%20bulk%20of%20the%20remaining,drilled%20almost%20a%20century%20ago).
- 1822
- 1823 Yuan, L., Stanley, A., Dehghanpour, H., & Reed, A. (2023). Measurement of helium
- 1824 diffusion in lotsberg salt cores: A proxy to evaluate hydrogen diffusion. *Inter-*
- 1825 *national Journal of Hydrogen Energy*. doi: 10.1016/j.ijhydene.2023.08.003
- 1826 Zahirovic, S., Matthews, K. J., Flament, N., Müller, R. D., Hill, K. C., Seton, M.,

- 1827 & Gurnis, M. (2016). Tectonic evolution and deep mantle structure of the
1828 eastern tethys since the latest jurassic. *Earth-Science Reviews*, *162*, 293-337.
1829 doi: 10.1016/j.earscirev.2016.09.005
- 1830 Zgonnik, V. (2020). The occurrence and geoscience of natural hydrogen: A com-
1831 prehensive review. *Earth-Science Reviews*, *203*. doi: 10.1016/j.earscirev.2020
1832 .103140
- 1833 Zhu, H., Li, X., & Xu, Y. (2020). A helium stratified and ingassed lower mantle: re-
1834 solving the helium paradoxes. *Acta Geochimica*, *39*, 4-10. doi: 10.1007/s11631
1835 -019-00378-2